

Kaluza-Klein Dark Matter: Direct Detection vis-a-vis LHC

Sebastian Arrenberg

Department of Physics, University of Zürich, Zürich, 8057, Switzerland

Laura Baudis

Department of Physics, University of Zürich, Zürich, 8057, Switzerland

Kyoungchul Kong

Fermi National Accelerator Laboratory, Batavia, IL 60510, USA

Konstantin T. Matchev

*Institute for Fundamental Theory, Physics Department,**University of Florida, Gainesville, FL 32611, USA*

Jonghee Yoo

Fermi National Accelerator Laboratory, Batavia, IL 60510, USA

(Dated: October 24, 2018)

Abstract

We explore the phenomenology of Kaluza-Klein (KK) dark matter in very general models with universal extra dimensions (UEDs), emphasizing the complementarity between high-energy colliders and dark matter direct detection experiments. In models with relatively small mass splittings between the dark matter candidate and the rest of the (colored) spectrum, the collider sensitivity is diminished, but direct detection rates are enhanced. UEDs provide a natural framework for such mass degeneracies. We consider both 5-dimensional and 6-dimensional non-minimal UED models, and discuss the detection prospects for various KK dark matter candidates: the KK photon γ_1 , the KK Z -boson Z_1 , the KK Higgs boson H_1 and the spinless KK photon γ_H . We combine collider limits such as electroweak precision data and expected LHC reach, with cosmological constraints from WMAP, and the sensitivity of current or planned direct detection experiments. Allowing for general mass splittings, we show that neither colliders, nor direct detection experiments by themselves can explore all of the relevant KK dark matter parameter space. Nevertheless, they probe different parameter space regions, and the combination of the two types of constraints can be quite powerful. For example, in the case of γ_1 in 5D UEDs the relevant parameter space will be almost completely covered by the combined LHC and direct detection sensitivities expected in the near future.

PACS numbers: 95.35.+d,11.10.Kk,12.60.-i,95.30.Cq,95.30.-k,14.80.Ly

I. INTRODUCTION

The Standard Model (SM) has been extremely successful in explaining all available experimental data in particle physics. However, there are several unsettling features of the SM, which have motivated a substantial research effort on physics beyond the Standard Model (BSM). The two issues continuously attracting the most attention are the hierarchy problem and the dark matter problem. The anticipated discovery of the Higgs boson of the SM at the Large Hadron Collider (LHC) at CERN would pose a challenging theoretical question: what is the next fundamental energy scale? If it is as high as the Planck scale, then what stabilizes the hierarchy between the Planck and electroweak scales? Or, if it is much lower than the Planck scale, what is the physics associated with it? The second issue is related to the now established existence of a dark matter (DM) component of the universe. Since the SM does not accommodate a suitable DM particle candidate, the dark matter problem is the most pressing phenomenological evidence for physics BSM [1].

A. The Dark Matter Problem and Physics Beyond the Standard Model

There are different avenues one could follow in extending the SM and addressing the dark matter problem. The common theme among them is the introduction of new particles, one of which is neutral and serves as the dark matter candidate; and a new symmetry, a remnant of which survives in the low energy effective theory and ensures that the lifetime of the DM particle is sufficiently long (at the minimum, longer than the age of the universe). In principle, simply postulating a new stable and neutral particle would be rather ad hoc and unsatisfactory without further corroborating evidence. Fortunately, the DM candidates in most BSM models typically have some kind of non-gravitational interactions, which are sufficient to keep them in thermal equilibrium in the early universe. Thus, their relic abundance can in fact be straightforwardly calculated in any given model (for details, see Section II B below). The generic result of this computation is that a weakly interacting massive particle (WIMP) with a mass near or below the TeV scale has a relic density in the right ballpark, and is a suitable candidate for dark matter. By now there are many examples of WIMPs in BSMs, perhaps the most popular being the lightest superpartner (LSP) in supersymmetry (SUSY) with R-parity conservation [2], the lightest Kaluza-Klein

partner (LKP) in Universal Extra Dimensions [3], the lightest T-parity odd particle in Little Higgs models [4, 5], the lightest U-parity odd particle in $U(1)'$ -extended models [6, 7], etc.

The most exciting aspect of the WIMP DM hypothesis is that it is testable by experiment. Indeed, WIMPs near the TeV scale can be easily within reach of both high-energy colliders and dark matter detection experiments. Furthermore, the size of the corresponding DM signals can be readily calculated within any given BSM, providing some rough expectations for discovery in each case. In principle, the signals depend on a typically a large number of model parameters. However, speaking in a broader sense, the WIMP DM phenomenology mostly depends on the answers to the following two questions:

- Q1: What is the identity of the DM particle candidate?
- Q2: What is the size of the mass splitting between the DM particle and the rest of the (relevant) spectrum?

In the following two subsections we shall discuss each one of these questions and thus motivate our setup and methodology.

B. The Nature of the Dark Matter Particle

Within any given BSM, there are typically several potential dark matter candidates (i.e. neutral and stable particles) present in the spectrum. The answer to the first question (Q1) therefore selects one of them as the “true” dark matter. For example, in SUSY, the dark matter particle could be either a fermion (e.g. gravitino or the lightest neutralino) or a boson (the lightest sneutrino). In turn, the lightest neutralino could be the superpartner of a gauge boson (e.g. a Bino, a Wino, possibly a Z' -ino), the superpartner of a Higgs boson (e.g. a Higgsino or a singlino) or some admixture of these [2]. Similarly, the lightest sneutrino could carry any one of the three lepton flavors, and in addition, could be left-handed [8], right-handed [9], or some mixture of both [10]. Since all of these particles have rather different properties, it is clear that it is impossible to make any generic predictions about SUSY dark matter without specifying the exact nature of the LSP, i.e. providing the answer to Q1 above.

On the positive side, the answer to Q1 goes a long way towards the determination of the size of the expected dark matter signals. Once the identity of the dark matter particle

is specified, its couplings are fixed and can be used in the calculation of both direct and indirect detection rates. What is even better, the answer to question Q1 can be provided in a rather model-independent way, without reference to the exact specifics of the model, such as the physics of the ultraviolet completion, Renormalization Group Equation (RGE) evolution down from high scales, etc.

In this paper, we shall explore the dark matter phenomenology of general models with flat universal extra dimensions [11], where the usual Standard Model structure is embedded in 5 or 6 space-time dimensions. We shall assume the same gauge symmetry and particle content as in the SM. Similar to the SUSY case just discussed, the models contain several possible dark matter candidates (electrically-neutral particles which are stable due to KK parity conservation)¹. In five dimensional models with minimal particle content, they are: the KK graviton (G_1), the KK neutrino (ν_1), the KK photon (γ_1), the KK Z -boson (Z_1) and the KK Higgs boson (H_1). Six dimensional UED models present additional possibilities: the spinless KK photon (γ_H) and the spinless KK Z -boson (Z_H), which are linear combinations of the gauge boson polarizations along the two extra dimensions. Just like the case of SUSY, which of these particles is the lightest and thus the dark matter candidate, depends on the model-building details. The issue is even more subtle than in SUSY, since all of these KK particles have tree-level masses of the same order, proportional to the inverse radius R^{-1} of the extra dimension. This mass degeneracy is lifted by two main sources: radiative corrections due to renormalization and nonuniversality in the boundary conditions at the cut-off scale. The former effect is in principle computable within any given model [12, 13, 14], while the latter is a priori unknown, as its origin lies in the ultraviolet physics above the cut-off scale [14, 15, 16, 17]. A common assumption throughout the existing literature on UED is to ignore any boundary terms at the cut-off scale. The resulting model has been dubbed “Minimal UED” and is known to accommodate only γ_1 and G_1 LKP in five dimensions [14, 18] and γ_H in six dimensions [19, 20]. However, given our complete ignorance of the physics at and above the cut-off scale, the other possibilities for the nature of the KK dark matter particle should be given serious consideration as well.

One of the goals of this paper is to start filling these gaps in the literature, by exploring the phenomenology of the alternative dark matter candidates in UED. Of course, not all of

¹ For further details on UED models, see Section II A.

them are on an equal footing. For example, the KK graviton G_1 interacts with the Standard Model particles too weakly to be relevant for direct detection searches. The KK neutrino ν_1 is already ruled out due to its large elastic scattering cross section [21]. We shall therefore concentrate on the remaining two possibilities in 5D UEDs: the KK Z -boson (Z_1) and the KK Higgs boson (H_1). We shall also review and update the previously published results on γ_1 and γ_H , so that our work would provide a concrete and complete reference on KK dark matter.

C. The Effect of a Mass Degeneracy on Dark Matter Signals

The second important issue for dark matter phenomenology is the answer to question Q2, namely, what is the mass splitting between the dark matter particle and the rest of the spectrum. Of course, it is in principle possible to have the dark matter particle as *the only* new particle in the model, in which case Q2 does not apply, and the predictions for the dark matter signals are quite robust, once Q1 is addressed. However, realistic models typically contain a multitude of new particles, in addition to the dark matter candidate. Their proximity (in mass) to the dark matter particle therefore becomes an important issue, at least in three, very different aspects.

The first is related to the predicted dark matter relic abundance. A close mass degeneracy can increase the importance of coannihilation processes at freeze-out [22], and the results for the relic density are now sensitive not only to the properties of the dark matter particle itself, but also to the properties of the coannihilating particles. The size of the coannihilation effect depends on the particular scenario, and there are several known cases in which it can be significant, e.g. Bino-like neutralinos in supersymmetry. The calculation of the relic density in the presence of coannihilations is a bit more involved (due to the larger number of processes which need to be considered), but nevertheless pretty straightforward. For UED models, where mass degeneracies are generically expected, the complete set of coannihilation processes which are relevant for the γ_1 and Z_1 LKP case in 5D UED have been calculated [21, 23, 24]. We shall make use of them in our analysis below in Section II B. After reviewing the case of γ_1 LKP, which has been previously discussed in the context of minimal UED, we shall also consider Z_1 LKP and illustrate the effects of coannihilations with KK quarks on its relic abundance. Since a calculation of coannihilations in 6D UED models is still lacking,

there we shall consider only one specific example in detail – the previously discussed case of γ_H [25]. The corresponding results for the direct detection rates of Z_H can be obtained by a simple scaling of the gauge couplings.

A small mass splitting also has a large impact on the expected direct detection signals, whenever the particle degenerate with the LKP can be exchanged in an s -channel. This situation may in principle arise in supersymmetry, if the squarks are very light, but this would be viewed by most people as a fortuitous accident. On the other hand, such a degeneracy occurs much more naturally in UED, where the masses of the KK quarks and the LKP necessarily have a common origin (the scale of the extra dimension). The mass degeneracy may lead to a substantial enhancement of the LKP elastic scattering rate [26]. In Section II C we first review the calculation of the spin-independent and the spin-dependent elastic scattering cross sections for the γ_1 LKP case [26]. Then we also consider the case of Z_1 , H_1 and γ_H LKP, paying special attention to the enhancement of the cross sections in the limit of small mass splittings.

Finally, the mass splitting between the dark matter candidate and the rest of the new physics spectrum is an important parameter for collider searches as well. The discovery reach for new physics at colliders is greatly diminished if the mass splittings are small. This is because the *observable* energy in the detector would then be rather small as well, in spite of the large amount of energy present in the events. Correspondingly, the *measured* missing energy (and any related variable such as H_T) is also rather small, which makes it more difficult to extract the new physics signal from the SM backgrounds. Fortunately, as mentioned above, this is precisely the case when direct detection is more promising. In Sec IV we shall explore this complementarity for various KK DM scenarios, focusing on KK gauge boson dark matter. From the previous discussion it should be clear that having specified the nature of the DM particle, the two most relevant parameters are the DM particle mass m_χ and the mass splitting with the nearest heavier colored particles. In Sec IV we shall utilize this two-dimensional parameter space, and contrast constraints from different sources: colliders, cosmological observations, and current or planned direct detection experiments (the latter are first extensively reviewed in Sec. III). As expected, we find that colliders and dark matter searches are highly complementary, while the WMAP constraint is orthogonal to them but is somewhat more model-dependent. Section V is reserved for a summary and conclusions. In the appendix we write out some technical details of our analysis.

II. UNIVERSAL EXTRA DIMENSIONS AND KALUZA-KLEIN DARK MATTER

A. Review on Universal Extra Dimensions

Models with universal extra dimensions place all Standard Model particles in the bulk of one or more compactified flat extra dimensions. In the simplest and most popular version, there is a single extra dimension compactified on an interval, S_1/Z_2 . In UED, each SM particle has a whole tower of KK modes. The individual modes are labelled by an integer n , called KK number, which is nothing but the number of quantum units of momentum which the SM particle carries along the extra dimension. A peculiar feature of UED is the conservation of Kaluza-Klein number at tree level, which is a simple consequence of momentum conservation along the extra dimension.

However, the fixed points in orbifold compactifications break translation invariance along the extra dimension. As a result, KK number is broken by bulk and brane radiative effects [12, 13, 14] down to a discrete conserved quantity, the so called KK parity $(-1)^n$. The geometrical origin of KK parity in the simplest (S_1/Z_2) case is the invariance under reflections with respect to the center of the interval. Since KK parity is conserved, the lightest KK parity odd particle is a suitable WIMP candidate [14, 21, 26, 27]. KK parity also ensures that the KK-parity odd KK partners (e.g. those at level one) are always pair-produced in collider experiments. This is reminiscent of the case of supersymmetry models with conserved R -parity. Therefore, the limits on UED KK modes from collider searches are relatively weak and are rather similar to the limits on superpartners. KK-parity is also responsible for weakening the potential indirect limits on UED models from low-energy precision data. Just like SUSY models with R-parity, the virtual effects from new physics only appear at the loop level and are loop suppressed [28, 29, 30].

Since all KK modes carry momentum along the extra dimension, at tree-level their masses receive a dominant contribution $\frac{n}{R} \sim n$ TeV, and a subdominant contribution from the corresponding SM particle mass. All KK modes at a given KK level n are therefore quite degenerate. The KK modes of the lightest SM particles (photons, leptons, light quarks) even appear to be absolutely stable *at tree level*. However, this conclusion is invalidated after accounting for the radiative corrections to the KK masses. The latter are proportional to $\frac{n}{R}$ and are sufficient to lift the degeneracy between the lightest KK modes, leaving only

one of them (the true LKP) as absolutely stable [14].

The nature of the LKP, on the other hand, is more model-dependent. In the minimal 5D UED model, where the boundary terms at the cut-off scale are ignored, the lightest KK particle is typically the $n = 1$ mode B_1 of the hypercharge gauge boson [14]. Since the Weinberg angle for the level one neutral gauge bosons is rather small, B_1 is essentially also a mass eigenstate, the KK “photon”, and we shall therefore denote it as γ_1 . The KK photon γ_1 is an attractive dark matter candidate [21, 26], whose relic abundance is consistent with the observed dark matter density for a mass range between 500 GeV and about 1.5 TeV, as shown by detailed computations including coannihilations [23, 24] and level-2 resonances [31, 32, 33]. Direct detection of this KK dark matter may be within reach of the next generation experiments [26, 34, 35, 36]. Indirect detection of KK dark matter also has better prospects than the case of neutralinos in SUSY [26, 37, 38, 39, 40, 41, 42, 43, 44].

In UED the bulk interactions of the KK modes readily follow from the Standard Model Lagrangian and contain no unknown parameters other than the mass m_h of the Standard Model Higgs boson. In contrast, the boundary interactions, which are localized on the orbifold fixed points, are in principle arbitrary, and thus correspond to new free parameters in the theory. They are in fact renormalized by bulk interactions, and are scale dependent [12]. Therefore, we need an ansatz for their values at a particular scale. Virtually all existing studies of UED have been done within the framework of minimal UED (MUED), in which the boundary terms are assumed to vanish at the cut-off scale Λ , and are subsequently generated through RGE evolution to lower scales (see [14, 45] for 5D and [19, 20] for 6D). In the minimal UED model therefore there are only two input parameters: the size of the extra dimension R , and the cut-off scale Λ . Of course, there are no compelling reasons for assuming vanishing boundary terms: the UED model should be treated only as an effective theory which is valid up to the high scale Λ , where it is matched to some more fundamental theory, which is generically expected to induce nonzero boundary terms at the matching scale Λ . As already mentioned in the introduction, nonvanishing boundary terms may change both the nature of the LKP, as well as the size of the KK mass splittings. The resulting phenomenology may be very different from the minimal case. This is why in this paper we shall allow for more general scenarios with Z_1 and H_1 LKP². In each case, we shall

² Other dark matter candidates, such as the level-1 KK mode of the graviton or of a right-handed neutrino,

take the LKP mass m_{LKP} and the LKP - KK quark mass splitting

$$\Delta_{q_1} = \frac{m_{q_1} - m_{LKP}}{m_{LKP}}, \quad (1)$$

as free parameters. We remind the reader that after compactification, the low energy effective theory contains two massive (Dirac) KK fermions for each (Dirac) fermion in the Standard Model. The KK fermions are properly referred to as $SU(2)_W$ -doublet KK fermions or $SU(2)_W$ -singlet KK fermions. However, in the literature they are sometimes called “left handed” and “right handed”, referring to the chirality of the corresponding Standard Model fermion at the zero level of the KK tower. This nomenclature may lead to some confusion, since all KK fermions are Dirac and have both chiralities. In our study, we shall treat the $SU(2)_W$ -doublet KK quarks (often denoted by Q_1) and the $SU(2)_W$ -singlet KK quarks (often denoted by q_1) equally, thus avoiding the need for two separate mass splitting parameters (for example, a separate Δ_{Q_1} and Δ_{q_1}). The generalization to the case of different KK quark masses is rather straightforward.

We shall also explore cases with more than one universal extra dimension. Theories with two universal extra dimensions also contain a KK parity. Under the simplest compactification which leads to chiral zero-mode fermions (a “chiral” square with adjacent sides identified [51, 52]), the KK parity transformations are reflections with respect to the center of the square. Momentum along the two compact dimensions is quantized so that any 6-dimensional field propagating on the square appears as a set of 4-dimensional particles labelled by two positive integers, (n, m) . These particles are odd under KK parity when $n + m$ is odd and are even otherwise. In any process, odd particles may be produced or annihilated only in pairs. The lightest odd particle, which is one of the $(1, 0)$ states, is thus stable. Gauge bosons propagating in six dimensions may be polarized along the two extra dimensions. As a result, for each spin-1 KK particle associated with a gauge boson, there are two spin-0 KK fields transforming in the adjoint representation of the gauge group. One linear combination becomes the longitudinal degree of freedom of the spin-1 KK particle, while the other linear combination remains as a physical spin-0 particle, called

are also viable for certain ranges of parameters in models with one universal extra dimension [18, 46, 47, 48, 49, 50].

the spinless adjoint³. In the minimal model with vanishing boundary terms, the radiative corrections [19, 20], are such that the lightest (1,0) particle on the chiral square [51, 52] is always a linear combination of the electrically-neutral spinless adjoints of the electroweak gauge group. Due to the small mixing angle, this linear combination is essentially a photon polarized along the extra dimensions. Similar to its 5D cousin γ_1 , the spinless photon γ_H in 6D UED is also a viable dark matter candidate [25]. See Refs. [53, 54, 55] for KK dark matter candidates in UED models with an extended gauge symmetry.

B. Relic Density Calculation with Coannihilations

We briefly review the calculation of the relic density including coannihilation processes. When the relic particle χ is nearly degenerate with other particles in the spectrum, its relic abundance is determined not only by its own self-annihilation cross section, but also by annihilation processes involving the heavier particles. The generalization of the relic density calculation including this “coannihilation” case is straightforward [21, 22]. Assume that the particles χ_i are labelled according to their masses, so that $m_i < m_j$ when $i < j$. The number densities n_i of the various species χ_i obey a set of Boltzmann equations. It can be shown that under reasonable assumptions [22], the ultimate relic density n_χ of the lightest species χ_1 (after all heavier particles χ_i have decayed into it) obeys the following simple Boltzmann equation

$$\frac{dn_\chi}{dt} = -3Hn_\chi - \langle \sigma_{eff} v \rangle (n_\chi^2 - n_{eq}^2) , \quad (2)$$

where H is the Hubble parameter, v is the relative velocity between the two incoming particles, n_{eq} is the equilibrium number density and

$$\sigma_{eff}(x) = \sum_{ij}^N \sigma_{ij} \frac{g_i g_j}{g_{eff}^2} (1 + \Delta_i)^{3/2} (1 + \Delta_j)^{3/2} \exp(-x(\Delta_i + \Delta_j)) , \quad (3)$$

$$g_{eff}(x) = \sum_{i=1}^N g_i (1 + \Delta_i)^{3/2} \exp(-x\Delta_i) , \quad (4)$$

$$\Delta_i = \frac{m_i - m_1}{m_1} , \quad x = \frac{m_1}{T} . \quad (5)$$

³ In contrast to the 6D case, KK particles in 5D UED are labelled by only one integer and spinless adjoints do not exist since there is only one gauge boson degree of freedom polarized along the extra dimension.

Here $\sigma_{ij} \equiv \sigma(\chi_i \chi_j \rightarrow SM)$ are the various pair annihilation cross sections into final states with SM particles, g_i is the number of internal degrees of freedom of particle χ_i and $n_\chi \equiv \sum_{i=1}^N n_i$ is the density of χ_1 we want to calculate.

By solving the Boltzmann equation analytically with appropriate approximations [21, 22], the abundance of the lightest species χ_1 is given by

$$\Omega_\chi h^2 \approx \frac{1.04 \times 10^9 \text{ GeV}^{-1}}{M_{Pl}} \frac{x_F}{\sqrt{g_*(x_F)}} \frac{1}{I_a + 3I_b/x_F} , \quad (6)$$

where the Planck mass scale is $M_{Pl} = 1.22 \times 10^{19} \text{ GeV}$ and g_* is the total number of effectively massless degrees of freedom at temperature T :

$$g_*(T) = \sum_{i=bosons} g_i + \frac{7}{8} \sum_{i=fermions} g_i . \quad (7)$$

The functions I_a and I_b are defined as

$$I_a = x_F \int_{x_F}^{\infty} a_{eff}(x) x^{-2} dx , \quad (8)$$

$$I_b = 2x_F^2 \int_{x_F}^{\infty} b_{eff}(x) x^{-3} dx . \quad (9)$$

The freeze-out temperature, x_F , is found iteratively from

$$x_F = \ln \left(c(c+2) \sqrt{\frac{45}{8}} \frac{g_{eff}(x_F)}{2\pi^3} \frac{m_1 M_{Pl} (a_{eff}(x_F) + 6b_{eff}(x_F)/x_F)}{\sqrt{g_*(x_F)} x_F} \right) , \quad (10)$$

where the constant c is determined empirically by comparing to numerical solutions of the Boltzmann equation and here we take $c = \frac{1}{2}$ as usual. a_{eff} and b_{eff} are the first two terms in the velocity expansion of σ_{eff}

$$\sigma_{eff}(x) v = a_{eff}(x) + b_{eff}(x) v^2 + \mathcal{O}(v^4) . \quad (11)$$

Comparing Eqns. (3) and (11), one gets

$$a_{eff}(x) = \sum_{ij}^N a_{ij} \frac{g_i g_j}{g_{eff}^2} (1 + \Delta_i)^{3/2} (1 + \Delta_j)^{3/2} \exp(-x(\Delta_i + \Delta_j)) , \quad (12)$$

$$b_{eff}(x) = \sum_{ij}^N b_{ij} \frac{g_i g_j}{g_{eff}^2} (1 + \Delta_i)^{3/2} (1 + \Delta_j)^{3/2} \exp(-x(\Delta_i + \Delta_j)) , \quad (13)$$

where a_{ij} and b_{ij} are obtained from $\sigma_{ij}v = a_{ij} + b_{ij}v^2 + \mathcal{O}(v^4)$ and v is the relative velocity between the two annihilating particles in the initial state. Considering relativistic corrections [56] to the above treatment results in an additional subleading term which can be accounted for by the simple replacement

$$b \rightarrow b - \frac{1}{4}a , \quad (14)$$

in the above formulas. For our calculation of the relic density, we use the cross sections given in Refs. [21, 23, 24].

As explained earlier, the assumptions behind MUED can be easily relaxed by allowing nonvanishing boundary terms at the scale Λ [15, 16, 17, 45]. This would modify the KK spectrum and correspondingly change the MUED predictions for the KK relic density. Within the modified KK spectrum, any neutral KK particle could be a dark matter candidate. As an illustration here we shall consider the case of γ_1 and Z_1 LKP⁴, for which the results for the relevant coannihilation processes are available in the literature [23, 24]. In Fig. 1, we show the relic densities of γ_1 and Z_1 as a function of the corresponding LKP mass (m_{γ_1} or m_{Z_1}) in 5D UED. We include coannihilation effects with all $n = 1$ KK particles with properly defined masses. The (black) solid lines show the LKP relic density for several choices of the mass splitting (1) between the LKP and the KK quarks. We assume that singlet and doublet KK quarks are degenerate (i.e., $\Delta_{Q_1} = \Delta_{q_1}$). The green horizontal band denotes the preferred 2σ -WMAP region for the relic density $0.1037 < \Omega_{CDM}h^2 < 0.1161$ [58]. The cyan vertical band delineates values of m_{LKP} disfavored by precision data [59, 60]⁵. In each case of Fig. 1a, we use the MUED spectrum to fix the masses of the remaining particles, and

⁴ The Z_1 is also a good dark matter candidate in warped extra dimensions with KK parity [57].

⁵ While there have been no studies of non-minimal UED models with Z_1 LKP, we anticipate that the precision bounds in that case will be similar to those in MUED, therefore we display the same indirect constraint in Fig. 1b.

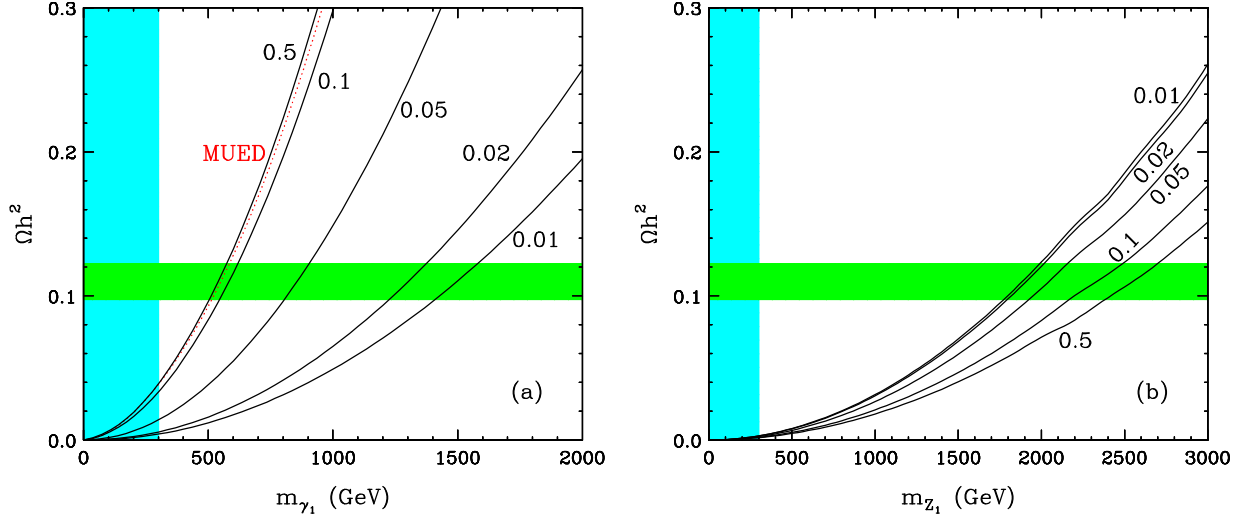


FIG. 1: Relic density of the LKP ((a) γ_1 and (b) Z_1) as a function of the LKP mass. The (black) solid lines show the LKP relic density for several choices of the mass splitting (1) between the LKP and the KK quarks. We assume that singlet and doublet KK quarks are degenerate. The green horizontal band denotes the preferred WMAP region for the relic density $0.1037 < \Omega_{CDM}h^2 < 0.1161$. The cyan vertical band delineates values of m_{LKP} disfavored by precision data. (a) We vary the q_1 mass by hand, keeping the masses of the remaining particles fixed as in MUED. The solid lines from top to bottom correspond to $\Delta_{q_1} = 0.5, 0.1, 0.05, 0.02, 0.01$. The (red) dotted line is the result from the full calculation in MUED, including all coannihilation processes, with the proper MUED choice for all masses. (b) We assume Z_1 and W_1^\pm are degenerate, the gluon is heavier than Z_1 by 20%, while all other KK particles are heavier than Z_1 by 10%. The solid lines from top to bottom correspond to $\Delta_{q_1} = 0.01, 0.02, 0.05, 0.1, 0.5$.

then vary the (common) KK-quark mass m_{q_1} by hand. The solid lines from top to bottom correspond to $\Delta_{q_1} = 0.5, 0.1, 0.05, 0.02, 0.01$. The (red) dotted line is the result from the full calculation in MUED, including all coannihilation processes, with the proper MUED choice for all masses. In Fig. 1b we assumed Z_1 and W_1^\pm are degenerate, the gluon is heavier than Z_1 by 20%, while all other KK particles are heavier than Z_1 by 10%. The solid lines from top to bottom correspond to $\Delta_{q_1} = 0.01, 0.02, 0.05, 0.1, 0.5$. Some individual quantities entering the relic density calculation for γ_1 (Z_1) LKP are shown in Fig. 2 (Fig. 3).

We see that coannihilations in the case of γ_1 LKP decrease the prediction for Ωh^2 and therefore increase the range of preferred m_{γ_1} values. For Δ_{q_1} on the order of a few percent, the desired range of m_{γ_1} is pushed beyond 1 TeV. This poses a challenge for any collider searches for UED, since the KK production cross sections at the LHC become kinematically suppressed for heavier KK modes. What is even worse, the small mass splitting Δ_{q_1} degrades the quality of the discovery signatures, e.g. the cascade decays of the KK quarks would yield

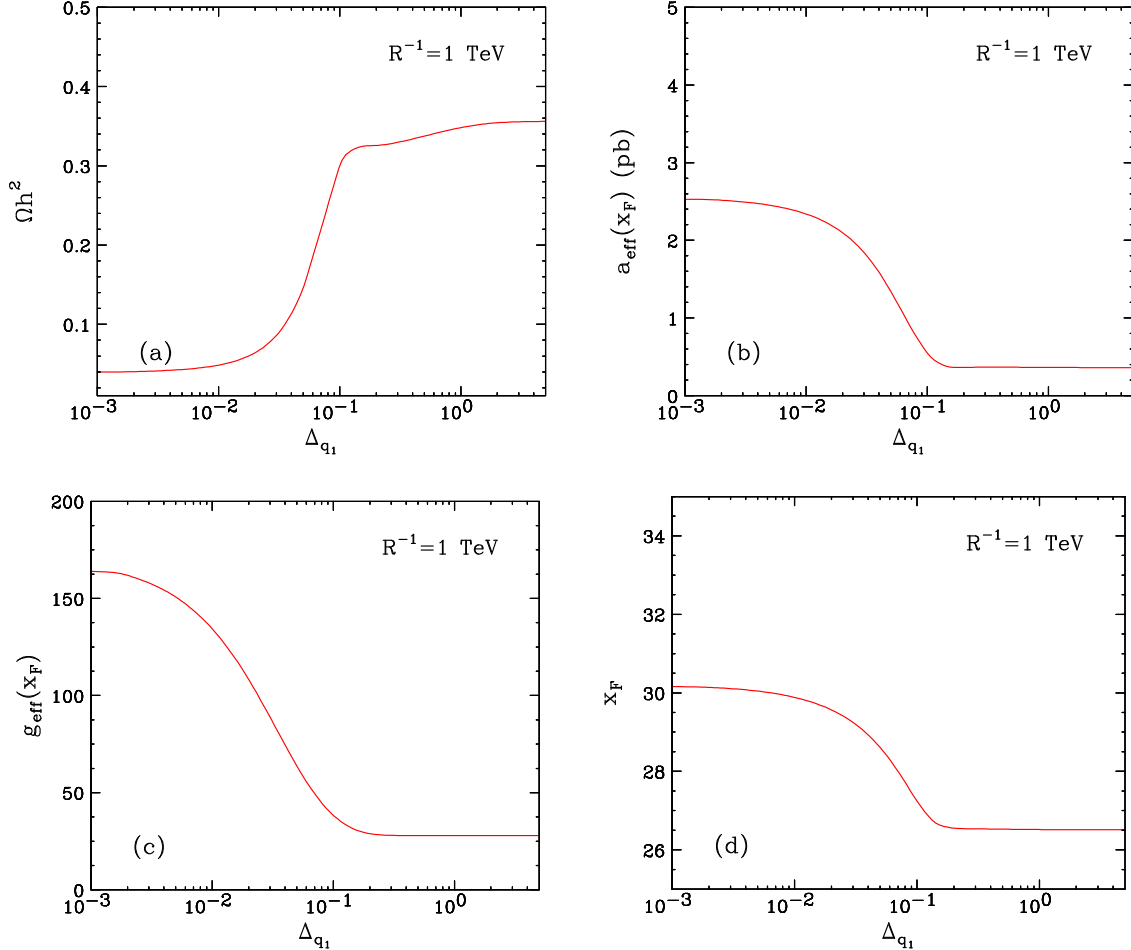


FIG. 2: Plots of various quantities entering the γ_1 LKP relic density computation, as a function of the mass splitting Δ_{q_1} between the LKP and the KK quarks: (a) relic density, (b) $a_{eff}(x_F)$, (c) $g_{eff}(x_F)$, and (d) x_F . In all four panels, the KK quark masses are varied by hand according to the value of Δ_{q_1} , while the masses of the γ_1 and the remaining KK modes are held fixed at their nominal values predicted in MUED for $R^{-1} = 1$ TeV.

only (rather soft) jets and no leptons.

On the other hand, Fig. 1b reveals that coannihilations with KK quarks have the opposite effect in the case of Z_1 LKP⁶. This time the effect of coannihilations is to increase the prediction for Ωh^2 and thus lower the preferred range of values for m_{Z_1} . The lesson from Figs. 1a and 1b is that while coannihilations can be quite important, the sign of the effect cannot be easily predicted, since, as will be illustrated in Figs. 2 and 3, it depends on the detailed balance of several numerical factors entering the computation. We shall discuss

⁶ A similar behavior exists in the case of γ_1 LKP when coannihilations are caused by the $SU(2)$ -singlet KK leptons ℓ_{R1} [21, 23, 24].

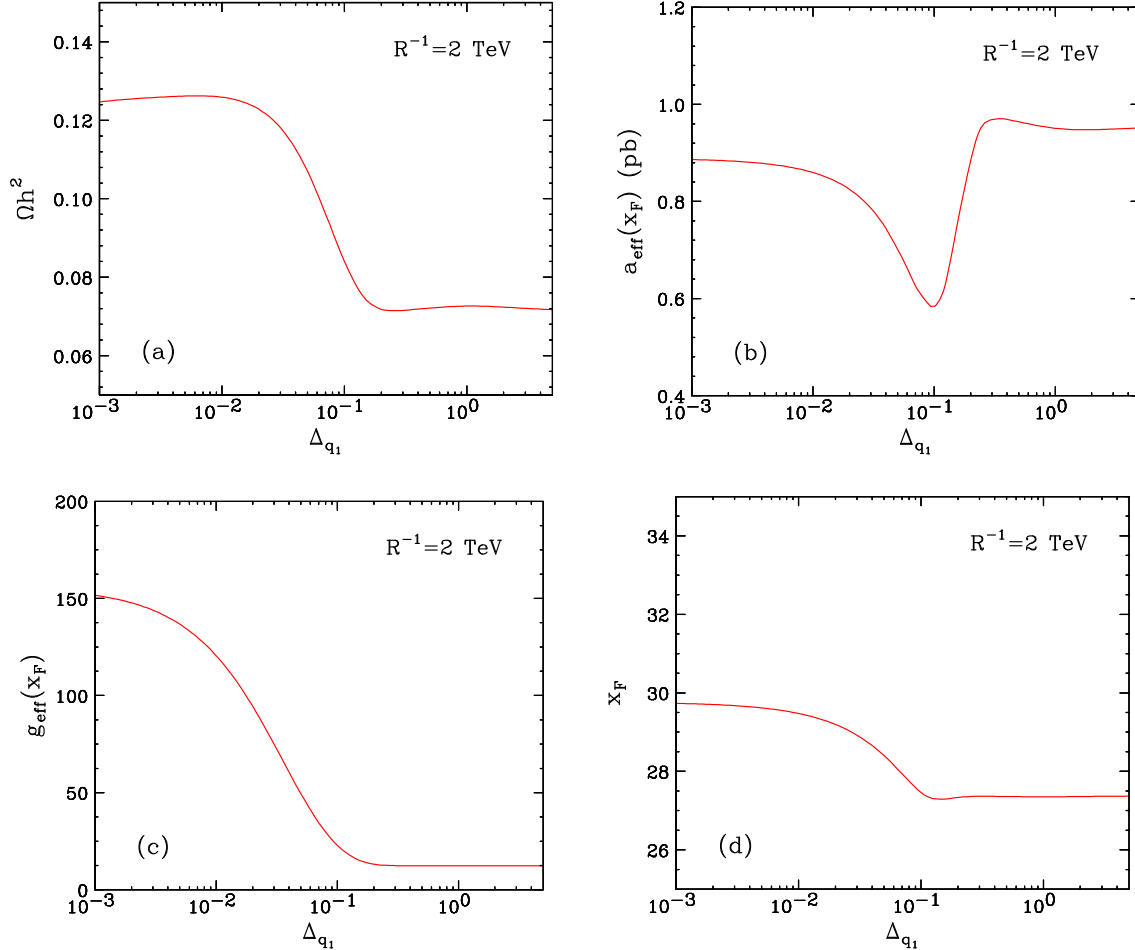


FIG. 3: The same as Fig. 2 but for Z_1 LKP. Here the Z_1 and W_1^\pm masses are taken to be 2 TeV, the KK quark masses are varied in accordance with Δ_{q_1} , while the remaining spectrum is fixed as in Fig. 1b.

these in some detail in the remainder of this subsection. Readers who are not interested in these numerical details, are invited to jump to Section II C.

In Fig. 2a (Fig. 3a) we plot the relic density of the γ_1 (Z_1) LKP, as a function of the mass splitting Δ_{q_1} between the KK quarks and the corresponding LKP. The rest of the spectrum is held fixed as explained in the figure captions. Figs. 2a and 3a demonstrate the importance of coannihilations at small mass splittings. For Δ_{q_1} larger than about 10–20%, coannihilations are turned off, but for KK quarks within 10% of the LKP mass, the coannihilation effect is significant. For γ_1 LKP, it lowers the prediction for the relic density Ωh^2 , while in the case of Z_1 LKP Ωh^2 is enhanced. In order to understand this different behavior, it is sufficient to investigate the coannihilation effect on the effective cross section, and in particular the dominant term a_{eff} , which is plotted in Figs. 2b and 3b. As can be seen from eq. (12), every

term contributing to a_{eff} is a ratio between two quantities, each of which has a nontrivial Δ_{q_1} dependence. The denominator is common to all terms and is nothing but the effective number of heavy particle degrees of freedom g_{eff} defined in eq. (4). We show the g_{eff} dependence on Δ_{q_1} in Figs. 2c and 3c. As expected, g_{eff} increases significantly after the turn-on of coannihilations (below $\Delta_{q_1} \sim 0.1$), due to the large multiplicity of KK quark states. At the same time, the numerator of each term contributing to the a_{eff} sum (12) is simply the Boltzmann suppressed annihilation cross section, which also increases with the onset of coannihilations (at small mass splittings Δ_{q_1}). The net effect on a_{eff} is determined by which of these two quantities increases *faster* at small Δ_{q_1} , relative to the nominal case without coannihilations. In the case of γ_1 LKP, the self-annihilation cross sections are rather weak, due to the smallness of the hypercharge gauge coupling. Adding the contributions from the strongly interacting KK quark sector has therefore a much larger impact than the associated increase in the effective number of degrees of freedom g_{eff} . As a result, a_{eff} increases and Ωh^2 decreases, as shown in Figs. 2a and 2b. In contrast, in the case of Z_1 LKP, the self-annihilation cross sections by themselves are already larger, due to the larger value of the weak gauge coupling. The gain from the addition of the KK quark coannihilation processes is more than compensated by the associated increase in the effective number of degrees of freedom g_{eff} . As a result, in this case a_{eff} decreases and Ωh^2 increases, as shown in Figs. 3a and 3b.

In conclusion, we should mention that the KK Higgs boson H_1 in principle can also be a potential dark matter candidate. The calculation of its relic density is somewhat more model-dependent and we do not consider it here.

C. Elastic Scattering Cross Sections

The elastic scattering of the LKP on a nucleon is described by the diagrams depicted in Fig. 4. For γ_1 LKP, the corresponding results can be found in [26, 34]. We follow the

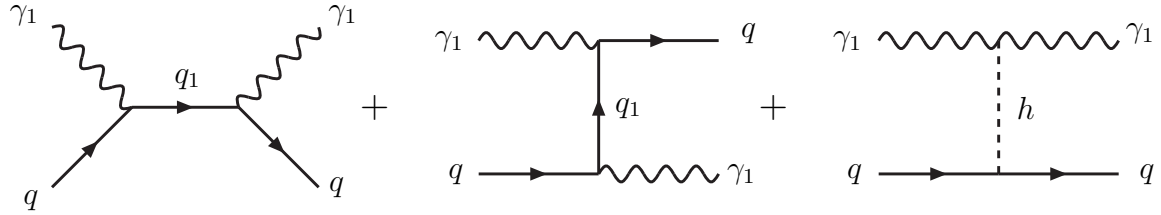


FIG. 4: Tree-level diagrams for the elastic scattering of γ_1 LKP with quarks. The diagrams for the case of Z_1 LKP are similar.

computation done in [26]⁷. The spin-independent cross section is given by

$$\sigma_{\text{scalar}} = \frac{m_T^2}{4\pi(m_{\gamma_1} + m_T)^2} [Zf_p + (A - Z)f_n]^2 , \quad (15)$$

where m_T is the mass of the target nucleus, Z and A are respectively the nuclear charge and atomic number, while

$$f_p = \sum_{u,d,s} (\beta_q + \gamma_q) \langle p | \bar{q}q | p \rangle = \sum_{u,d,s} \frac{\beta_q + \gamma_q}{m_q} m_p f_{T_q}^p , \quad (16)$$

and similarly for f_n . In eq. (16) m_p (m_n) stands for the proton (neutron) mass. For the nucleon matrix elements we take $f_{T_u}^p = 0.020 \pm 0.004$, $f_{T_d}^p = 0.026 \pm 0.005$, $f_{T_u}^n = 0.014 \pm 0.003$, $f_{T_d}^n = 0.036 \pm 0.008$, and $f_{T_s}^{p,n} = 0.118 \pm 0.062$ [61]. The numerical coefficients β_q and γ_q in eq. (16) are defined as⁸

$$\beta_q = \frac{e^2}{\cos^2 \theta_W} \left[E_q (Y_{qL}^2 \cos^2 \alpha + Y_{qR}^2 \sin^2 \alpha) \frac{m_{q_L^1}^2 + m_{\gamma_1}^2}{(m_{q_L^1}^2 - m_{\gamma_1}^2)^2} + \frac{Y_{qL} Y_{qR} m_{q_L^1} \sin 2\alpha}{m_{\gamma_1}^2 - m_{q_L^1}^2} + (L \rightarrow R) \right] \quad (17)$$

$$\approx E_q \frac{e^2}{\cos^2 \theta_W} \left[Y_{qL}^2 \frac{m_{\gamma_1}^2 + m_{q_L^1}^2}{(m_{q_L^1}^2 - m_{\gamma_1}^2)^2} + (L \rightarrow R) \right] \quad \text{for } \alpha = 0 , \quad (18)$$

$$\gamma_q = m_q \frac{e^2}{2 \cos^2 \theta_W} \frac{1}{m_h^2} , \quad (19)$$

⁷ The precise calculation of the heavy quark contribution to the processes of Fig. 4 is rather involved – the heavy flavors contribute only at the loop level, through the gluon content of the nucleon. In the absence of an exact calculation of these effects in the literature, we choose to conservatively ignore the heavy flavor contributions altogether, as was done in [26].

⁸ Ref. [34] contains a typo in the overall sign of the coefficient β_q , which was denoted there as S_q .

where e is the electric charge, θ_W is the Weinberg angle, $m_{q_L^1}$ ($m_{q_R^1}$) is the mass of an $SU(2)_W$ -doublet ($SU(2)_W$ -singlet) KK quark, and α is the mixing angle in the KK quark mass matrix given by $\sin 2\alpha = 2m_q/(m_{q_L^1} + m_{q_R^1})$. Eq. (17) includes the mixing effect between two KK quarks and eq. (18) is obtained in the limit when $\alpha = 0$. This mixing effect gives a minor correction to the cross section (at a few percent level) and we do not include it in our figures for 5D. However it is important to keep it in the 6D case, as shown in Ref. [25]. Our convention for the SM hypercharge is $Y_i = Q_i - I_{3i}$, where Q_i (I_{3i}) is the electric charge (weak isospin) of particle i . E_q in eq. (18) is the energy of a bound quark and is rather ill-defined. In evaluating eq. (16), we conservatively replace E_q by the current⁹ mass m_q . As alluded to earlier, in eq. (18) we only sum over light quark flavors, thus neglecting couplings to gluons mediated by heavy quark loops. Note that the two contributions (18) and (19) to the scalar interactions interfere constructively: even with extremely heavy KK quark masses (large Δ_{q_1}), there is an inescapable lower bound on the scalar cross section for a given Higgs mass, since the Higgs contribution from eq. (19) scales with the SM Higgs mass m_h and not the KK quark masses.

The analogous results for the case of Z_1 LKP can now be obtained from the above formulas by simple replacements: $m_{\gamma_1} \rightarrow m_{Z_1}$, $Y_{q_L} \rightarrow \frac{1}{2}$ and $Y_{q_R} \rightarrow 0$, since Z_1 is mostly the neutral $SU(2)_W$ gauge boson, which has no interactions with the $SU(2)_W$ -singlet KK quarks (or equivalently, the right-handed SM quarks). In addition, one should replace $\frac{e}{\cos \theta_W} \rightarrow \frac{e}{\sin \theta_W}$ to account for the different gauge coupling constant.

Theoretical predictions for the spin-independent LKP-nucleon elastic scattering cross sections are shown in Fig. 5 for different fixed values of the KK quark - LKP mass splitting Δ_{q_1} , and for two different LKPs: (a) γ_1 and (b) Z_1 . In both cases the cross sections decrease as a function of LKP mass. This is due to the inverse scaling of the KK quark exchange contributions (18) with the KK mass scale. Comparing Fig. 5a to 5b, we notice that the scalar cross section for Z_1 is more than one order of magnitude larger than the scalar cross section for γ_1 of the same mass. This is mostly due to the larger $SU(2)_W$ gauge coupling. Notice that even when the KK quarks are very heavy, there is still a reasonable cross section, which is due to the Higgs mediated contribution (19). Perhaps the most noteworthy feature

⁹ The actual choice of the value for m_q is inconsequential since the m_q factor in eqs. (18) and (19) cancels against the m_q factor in the denominator of eq. (16).

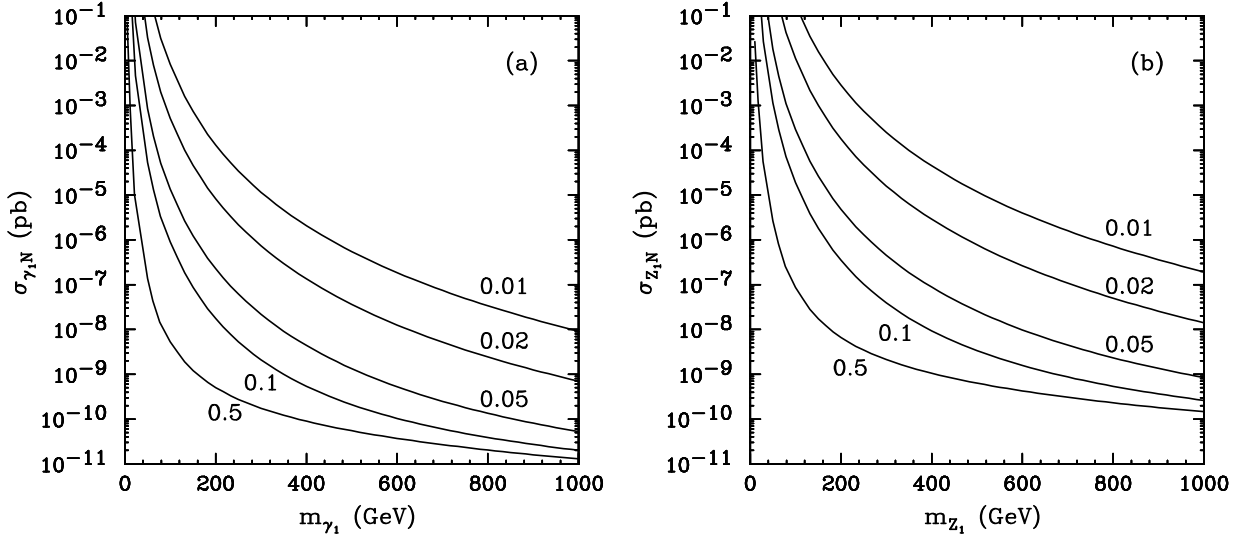


FIG. 5: *Spin-independent elastic scattering cross sections as a function of LKP mass for (a) γ_1 and (b) Z_1 . The individual curves are labelled by the value of the mass splitting Δ_{q_1} . The SM Higgs mass m_h is fixed to 120 GeV.*

of Figs. 5a and 5b is the significant enhancement of the direct detection signals at small Δ_{q_1} , often by several orders of magnitude. This greatly enhances the prospects for detecting KK dark matter, if the mass spectrum turns out to be rather degenerate.

The spin-dependent cross section is given by

$$\sigma_{\text{spin}} = \frac{1}{6\pi} \frac{m_T^2}{(m_{\gamma_1} + m_T)^2} J_N (J_N + 1) \left[\sum_{u,d,s} \alpha_q \lambda_q \right]^2, \quad (20)$$

where α_q and λ_q are

$$\alpha_q = \frac{2e^2}{\cos^2 \theta_W} \left[\frac{Y_{qL}^2 m_{\gamma_1}}{m_{q_L^1}^2 - m_{\gamma_1}^2} + (L \rightarrow R) \right], \quad (21)$$

$$\lambda_q = \Delta_q^p \langle S_p \rangle / J_N + \Delta_q^n \langle S_n \rangle / J_N. \quad (22)$$

Here J_N is the nuclear spin operator. $\Delta_q^{p,n}$ is given by $\langle p, n | S_q^\mu | p, n \rangle \equiv \Delta_q^{p,n} S_{p,n}^\mu$ and is the fraction of the nucleon spin carried by the quark q . We use $\Delta_u^p = \Delta_d^n = 0.78 \pm 0.02$, $\Delta_d^p = \Delta_u^n = -0.48 \pm 0.02$, and $\Delta_s^p = \Delta_s^n = -0.15 \pm 0.02$ [62]. $\langle S_{p,n} \rangle / J_N \equiv \langle N | S_{p,n} | N \rangle / J_N$ is the fraction of the total nuclear spin J_N that is carried by the spin of protons or neutrons. For scattering off protons and neutrons, λ_q reduces to Δ_q^p and Δ_q^n , respectively.

Following [63], we can rewrite eq. (20) in the form

$$\sigma_{\text{spin}} = \frac{32}{\pi} G_F^2 \mu^2 \frac{J_N + 1}{J_N} (a_p \langle S_p \rangle + a_n \langle S_n \rangle)^2, \quad (23)$$

where G_F is the Fermi constant and

$$\mu = \frac{m_T m_{\gamma_1}}{m_T + m_{\gamma_1}} \quad (24)$$

is the reduced mass, while the coefficients a_p and a_n are given by

$$\begin{aligned} a_{p,n} &= \frac{1}{8\sqrt{3}G_F m_{\gamma_1}} \sum_{u,d,s} \alpha_q \Delta_q^{p,n} \\ &= \frac{e^2}{4\sqrt{3}G_F \cos^2 \theta_W} \sum_{u,d,s} \left[\frac{Y_{q_L}^2}{m_{q_L^1}^2 - m_{\gamma_1}^2} + (L \rightarrow R) \right] \Delta_q^{p,n}. \end{aligned} \quad (25)$$

The main advantage of introducing the parameters a_p and a_n is that they encode all the theoretical model-dependence, thus allowing different experiments to compare their sensitivities in a rather model-independent way. From eqs. (23-24) it is clear that for any given target, the spin-dependent scattering rate depends on only three parameters: m_{γ_1} , a_p and a_n . Notice that in our setup there are only two relevant model parameters: m_{LKP} and Δ_{q_1} , therefore we will have a certain correlation between a_p and a_n , depending on the nature of the LKP¹⁰.

In Fig. 6 we show our result for the spin-dependent LKP elastic scattering cross sections off protons and neutrons for the case of (a) γ_1 and (b) Z_1 , for different mass splittings Δ_{q_1} . The red solid curves are the LKP-proton cross sections and the blue dotted curves are the LKP-neutron cross sections. All curves exhibit the same general trends as the corresponding spin-independent results from Fig. 5: the cross sections decrease with the KK mass scale, and are enhanced for small mass splittings Δ_{q_1} . One peculiar feature is that the proton and

¹⁰ In introducing the parameters a_p and a_n we have followed the convention of Ref. [63]. We should alert the reader that a different convention was used in Ref. [34], where $a_{p,n}$ was defined as $a_{p,n} = \sum_{u,d,s} [Y_{q_L}^2 + Y_{q_R}^2] \Delta_q^{p,n}$, so that a_p and a_n are pure numerical factors, e.g. $a_n = -0.139167$ and $a_p = 0.280833$ for γ_1 LKP, and $a_n = a_p = 0.0375$ for Z_1 LKP. However, this factorization can only be done in the special case of $\Delta_{Q_1} = \Delta_{q_1}$, and furthermore, the theoretical model dependence (through the KK quark masses) creeps back explicitly in the expression for the spin-dependent cross section.

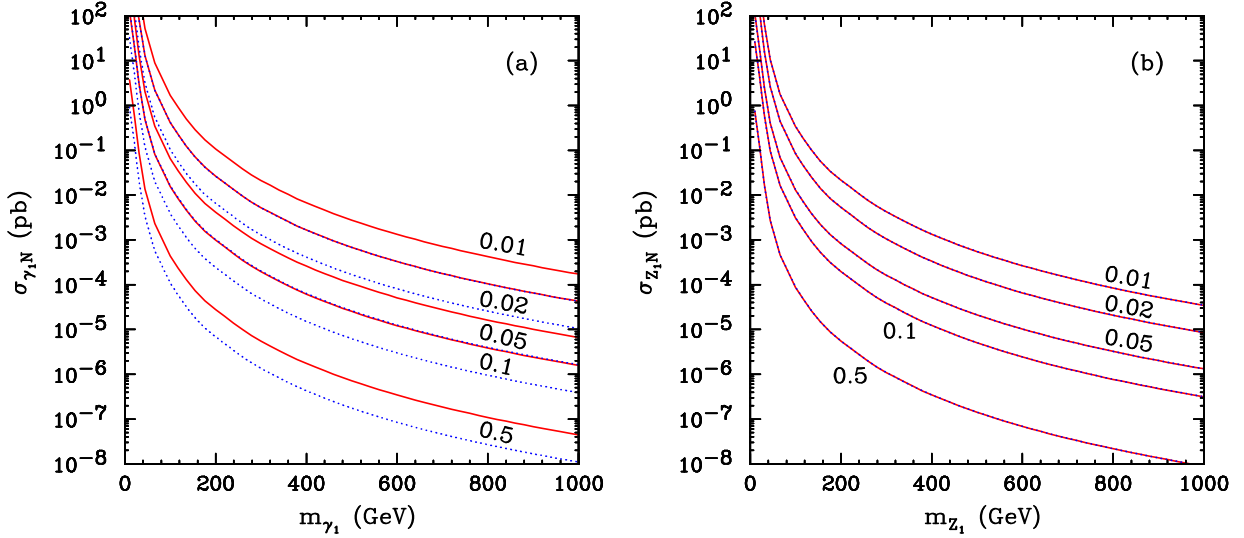


FIG. 6: The spin-dependent elastic scattering cross sections as a function of LKP mass for (a) γ_1 and (b) Z_1 at various Δ_{q_1} . The red solid curves are the LKP-proton cross sections and the blue dotted curves are the LKP-neutron cross sections. The LKP-proton and LKP-neutron cross sections are identical for Z_1 . For γ_1 the proton cross section is approximately 4 times larger than the neutron cross section, for the same values of the LKP mass m_{γ_1} and mass splitting Δ_{q_1} .

neutron spin-dependent cross sections are equal in the case of Z_1 , as seen in Fig. 6b. This is an exact statement, which is due to the fact that Z_1 does not particularly discriminate between the different quark flavors in the nucleon – it couples with equal strength to both up- and down-type (left-handed) quarks. On the other hand, γ_1 couples differently to u and d , because of the different hypercharges of the right-handed quarks. As a result, the cross sections on protons and neutrons differ in the case of γ_1 , as seen in Fig. 6a. Interestingly, for a given LKP mass m_{γ_1} and mass splitting Δ_{q_1} , the proton cross section in Fig. 6a is larger than the neutron cross section by about a factor of 4, which is due to a numerical coincidence involving the values of the quark hypercharges and the $\Delta_q^{p,n}$ parameters.¹¹ Because of this simple scaling, for a given LKP mass m_{γ_1} , the proton cross section at a certain Δ_{q_1} coincides with the neutron cross section for half the mass splitting ($\Delta_{q_1}/2$) since to leading order both the proton and the neutron cross sections are proportional to $(\Delta_{q_1})^{-2}$.

We shall now review the corresponding results for the case of two universal extra dimensions. The sum $\beta_q + \gamma_q$ for the spinless photon (γ_H) LKP was computed in [25] (note that

¹¹ This can be simply understood in terms of the relative scaling of the a_p and a_n parameters introduced in Eq. (23). In the case of γ_1 , they differ by a factor of -2, while for the case of Z_1 they are the same.

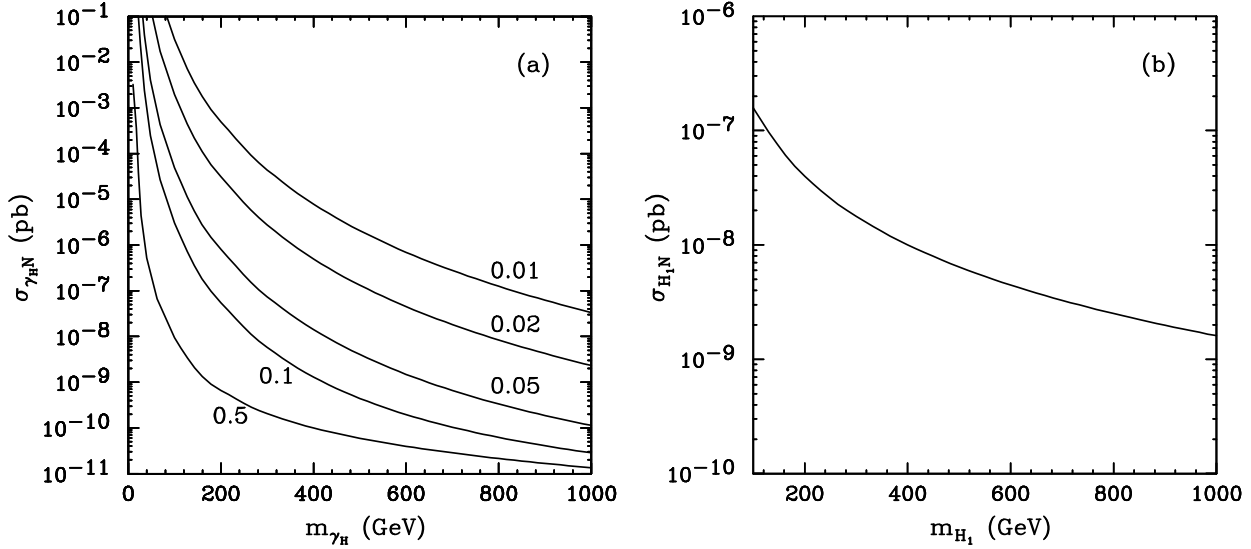


FIG. 7: The spin-independent elastic scattering cross sections as a function of LKP mass for (a) γ_H in 6D UED and (b) H_1 in 5D UED. In the case of γ_H LKP (panel “a”), we present results for several values of Δ_{q_1} as shown. In the case of H_1 (panel “b”), we only show the contribution from the SM Higgs exchange, assuming heavy KK quarks.

here we are using a different convention for the hypercharges Y_i)

$$\begin{aligned} \beta_q + \gamma_q = & \frac{e^2}{\cos^2 \theta_W} \left[m_q (Y_{qL} + Y_{qR})^2 \left(\frac{1}{m_{q1}^2 - (m_q - m_{\gamma_H})^2} + \frac{1}{m_{q1}^2 - (m_q + m_{\gamma_H})^2} \right) \right. \\ & \left. + m_{\gamma_H} (Y_{qL}^2 + Y_{qR}^2) \left(\frac{1}{m_{q1}^2 - (m_q + m_{\gamma_H})^2} - \frac{1}{m_{q1}^2 - (m_q - m_{\gamma_H})^2} \right) + \frac{m_q}{2m_h^2} \right], \end{aligned} \quad (26)$$

where m_{γ_H} is the mass of the spinless photon, m_{q1} is the (common) mass of the $SU(2)_W$ -doublet and $SU(2)_W$ -singlet KK quarks, while m_q is the corresponding SM quark mass.

Using Eqn. (15), we obtain the spin-independent elastic scattering cross section for γ_H as shown in Fig. 7a. The different curves are labelled by the assumed fixed value of Δ_{q_1} , and are plotted versus the LKP mass m_{γ_H} . We see that the size of the γ_H signal is about the same order as the γ_1 cross sections from Fig. 5a. On the other hand, the relic density constraint would single out somewhat different regions for m_{γ_1} and m_{γ_H} . The annihilation cross section for γ_H is smaller than that of γ_1 [25], and correspondingly, lower γ_H masses would be preferred, with enhanced prospects for direct detection¹². Notice that there is no

¹² One should keep in mind that mass splittings Δ_{q_1} as small as those shown in the plot mandate the inclusion of coannihilation processes with KK quarks in 6D UED, as we did previously in the case of γ_1 and Z_1 in 5D UED (see Fig. 1). Unfortunately the computation of coannihilations in 6D UED does not

spin-dependent cross section for γ_H since it is a scalar particle.

In conclusion of this section, we shall briefly discuss the scenario of KK Higgs (H_1) LKP. Just like γ_H , H_1 is a scalar and does not have spin-dependent interactions. Its spin-independent elastic scattering cross section can be readily computed following the procedure outlined earlier in this section and in the appendix. In this case, the KK quark exchange diagrams are also Yukawa suppressed, and the dominant among them is the s KK quark contribution. As in the γ_1 LKP case, the diagrams with KK quark exchange and SM Higgs exchange interfere constructively. Therefore, the SM Higgs exchange diagram by itself provides a conservative lower bound on the elastic scattering cross section, independent of the other details of the KK spectrum, and in particular, the KK quark masses. This absolute minimum of the cross section is plotted in Fig. 7b as a function of the LKP mass m_{H_1} . It is worth mentioning that this result is completely independent of the SM Higgs mass m_h . The contribution corresponding to (19) is given by

$$\gamma_q = \frac{3}{4} \frac{e^2}{\sin^2 \theta_W} \frac{m_q}{m_W^2}, \quad (27)$$

where m_W is the mass of the W^\pm boson. The coupling of the KK Higgs to the SM Higgs boson is the same as the triple Higgs coupling of the SM, which is proportional to m_h^2 . This m_h^2 dependence is exactly cancelled by the m_h^{-2} dependence of the SM Higgs propagator in the non-relativistic limit (see Eqn. (19)). Therefore the final cross section is indeed independent of the SM Higgs mass, and this fact remains true regardless of the values of the KK quark masses.

III. DIRECT WIMP DETECTION AND EXPERIMENTS

The detailed distribution of dark matter in our galaxy, and in particular in the local neighborhood, is not well constrained by current observations and high-resolution simulations. The standard assumption for its distribution is a cored, non-rotating isothermal spherical halo with a Maxwell-Boltzmann velocity distribution with a mean of 220 km/s, and escape velocity from the galactic halo of 544 km/s [64]. For the local density of dark

exist in the literature. In analogy with the case of γ_1 LKP in 5D UED, we expect the coannihilation effects to increase the preferred range of m_{γ_H} .

matter particles we assume $\rho=0.3 \text{ GeV/cm}^3$ [65].

The WIMP interaction signature in ultra-low-background terrestrial detectors [66] consists of nuclear recoils. Direct detection experiments attempt to measure the small ($<100 \text{ keV}$) energy deposited when a WIMP scatters from a nucleus in the target medium. The recoil energy of the scattered nucleus is transformed into a measurable signal, such as charge, scintillation light or lattice excitations, and at least one of the above quantities can be detected. Observing two signals simultaneously yields a powerful discrimination against background events, which are mostly interactions with electrons as opposed to WIMPs and neutrons, which scatter from nuclei. The WIMP interaction takes place in the non-relativistic limit, therefore the total cross section can be expressed as the sum of a spin-independent (SI) part (see Eqn. (15)), a coherent scattering with the whole nucleus, and of a spin-dependent (SD) part (see Eqn. (20)), which describes the coupling to the total nuclear spin [67].

Neutrons with energies in the MeV range can elastically scatter from nuclei and mimic a WIMP signal. Two methods are used to discriminate against the residual neutron background, which comes from (α, n) - and fission-reactions in materials and from interactions of cosmic muons with the rock and experimental shields. First, the SI WIMP-nucleus cross section is proportional to the atomic mass-squared of the nucleus, making the expected total WIMP interaction rate material dependent. Second, the mean free paths of WIMPs and MeV neutrons are exceedingly different (10^{10} m versus 8 cm in a typical WIMP target), allowing to directly constrain the neutron background from the ratio of observed single to multiple interaction events.

The experimental upper bounds of the SI cross section from direct detection experiments are WIMP-type independent and thus will not change if we consider different WIMP candidates. Similarly, the SD cross section limits can also be reinterpreted for various DM candidates. The only exception is a spin zero WIMP, such as γ_H in 6D UED, which does not have an axial-vector coupling with nuclei, hence no SD interaction is expected. We will extensively discuss the model dependence of the SD cross section in the next section.

In this study, we choose four direct detection experiments which demonstrated best experimental sensitivity to-date in various parts of the WIMP search parameter space. The CDMS experiment sets the best SI upper bound above a WIMP mass of 42 GeV [68], while XENON10 gives the most stringent upper bound on WIMP-neutron SD couplings [70] and

Experiments	Target	Total mass	Energy range	Location	Ref.
CDMS II	Ge(Si)	4.75 kg (1.1 kg)	10 keV – 100 keV	Soudan, USA	[68]
XENON10	Xe	15 kg	4.5 keV – 27 keV	Gran Sasso, Italy	[69]
KIMS	CsI	34.8 kg	3 keV – 11 keV	Yangyang, Korea	[71]
COUPP	CF ₃ I	1.5 kg	5 keV –	Fermilab, USA	[72]

TABLE I: Direct WIMP detection experiments considered in this study.

SI couplings below 42 GeV [69]. The KIMS [71] and COUPP [72] experiments show the best sensitivity for SD WIMP-proton couplings. As we shall see in the following section, the combined study of all four experiments strongly constrains the SD proton-neutron mixed coupling parameter space (the so called a_p - a_n parameter space, where a_p and a_n are the dark matter particle's couplings to protons and neutrons, respectively, see eq. (23)).

Table I summarizes the relevant characteristics of the four experiments such as target material, total mass, energy range considered for the WIMP search, and location. In this paper we either calculated the LKP limits based on published data (XENON10), or we obtained the data points for the cross section upper bounds from the collaboration (CDMS, KIMS and COUPP).

The CDMS experiment [68] is operated in the Soudan Underground Laboratory, USA. It uses advanced Z(depth)-sensitive Ionization and Phonon (ZIP) detectors, which simultaneously measure the ionization and athermal phonon signals after a particle interacts in the crystal. The ZIP detectors provide excellent event-by-event discrimination of nuclear recoils from the dominant background of electron recoils. The most stringent limits on spin-independent couplings with nucleons above a WIMP mass of 42 GeV comes from the first two CDMS-II five tower runs with a raw exposure of 397.8 kg-days in germanium. The null observation of a WIMP signal sets a WIMP-nucleon cross section upper bound of 6.6×10^{-8} pb (for a 60 GeV WIMP mass) and of 4.6×10^{-8} pb when the results are combined with previous CDMS results.

The SuperCDMS project [73, 74] is a three-phase proposal to utilize CDMS-style detectors with target masses growing from 25 kg to 150 kg and up to 1 ton, with the aim of reaching a final sensitivity of 3×10^{-11} pb by mid 2015. This goal will be realized by developing improved detectors and analysis techniques, and concomitantly reducing the intrinsic surface contamination of the crystals.

The XENON10 collaboration [69] operated a 15 kg active mass, dual-phase (liquid and

gas) xenon time projection chamber in the Gran Sasso Underground Laboratory (LNGS), in WIMP search mode from August 2006 to February 2007. XENON10 uses two arrays of UV-sensitive photomultipliers (PMTs) to detect the prompt and proportional light signals induced by particles interacting in the sensitive liquid xenon (LXe) volume. The 3D position sensitivity, the self-shielding of LXe and the prompt versus proportional light ratio are the most important background rejection features. The first results, using ~ 136 kg-days exposure after cuts, demonstrated that LXe can be used for stable, homogeneous, large scale dark matter detectors, providing excellent position resolution and discrimination against the electron recoil background. The derived upper bound on SI cross sections on nucleons is 4.5×10^{-8} pb for a WIMP mass of 30 GeV. Since natural Xe contains ^{129}Xe (26.4%) and ^{131}Xe (21.2%) isotopes, each of these having an unpaired neutron, the XENON10 results substantially constrain the SD WIMP-nucleon cross section. We calculated the XENON10 SD LKP-neutron and LKP-proton upper bounds based on the observation of 10 events, without any background subtraction [70]. The next phase, XENON100, will operate a total of 170 kg (70 kg fiducial) of xenon, viewed by 242 PMTs, in a dual-phase TPC in an improved XENON10 shield at the Gran Sasso Laboratory. While the fiducial mass is increased by more than a factor of 10, the background will be lower by about a factor of 100 (through careful selection of ultra-low background materials, the placing of cryogenic devices and high-voltage feed-throughs outside of the shield and by using 100 kg of active LXe shield) compared to XENON10. XENON100 is currently being commissioned at LNGS, the aim is to start the first science run in fall 2008, probing WIMP-nucleon SI cross sections down to $\sim 10^{-9}$ pb.

The Korea Invisible Mass Search (KIMS) experiment [71] is located at the Yangyang Underground Laboratory, Korea. The collaboration has operated four low-background CsI(Tl) crystals, each viewed by two photomultipliers, for a total exposure of 3409 kg-days. Both ^{133}Cs and ^{127}I are sensitive to the spin-dependent interaction of WIMPs with nuclei. KIMS detects the scintillation light after a particle interacts in one of the crystals, kept stably at $(0 \pm 0.1)^\circ\text{C}$. The pulse shape discrimination technique, using the time distribution of the signal, allows to statistically separate nuclear recoils from the electron recoil background. The KIMS results are consistent with a null observation of a WIMP signal, yielding the best limits on SD WIMP-proton couplings for a WIMP mass above 30 GeV. Specifically, the upper bound for a WIMP mass of 80 GeV is 1.7×10^{-1} pb.

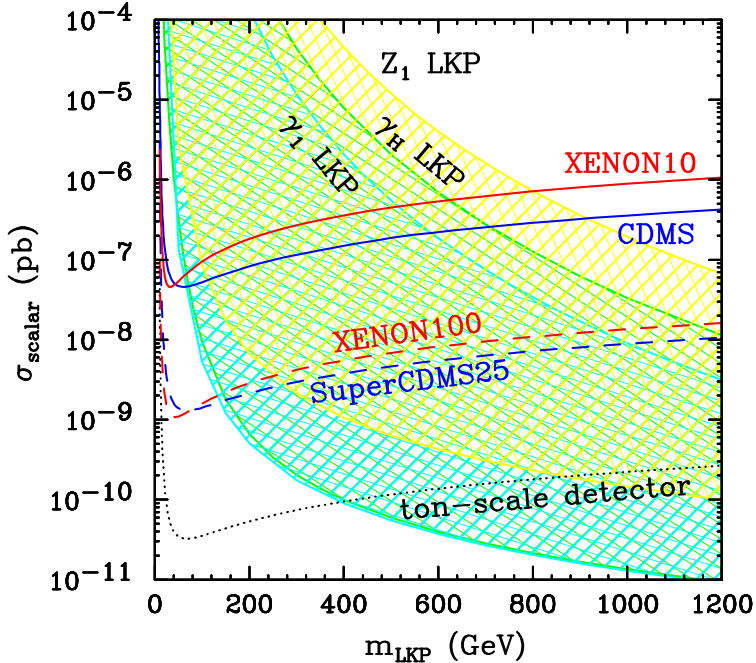


FIG. 8: *Current and projected experimental limits on the SI LKP-nucleon-scattering cross section together with the theoretically expected γ_1 (blue shaded), Z_1 (yellow shaded) and γ_H (green-shaded) LKP regions. The boundaries of the LKP regions are selected for $0.01 < \Delta < 0.5$ while the Higgs mass m_h is fixed to 120 GeV. The solid lines are the current experimental upper bounds (90% C.L) from the CDMS (blue) and XENON10 (red) experiments. The dashed lines are expected sensitivities for the SuperCDMS 25 kg (blue) and XENON100 (red) experiments, which will be operated in the near future. The dotted line is the expected sensitivity for a ton-scale detector.*

The Chicagoland Observatory for Underground Particle Physics (COUPP) experiment [72] is operated at Fermilab, USA. The experiment has revived the bubble chamber technique for direct WIMP searches. The superheated liquid can be tuned such that the detector responds only to keV nuclear recoils, being fully insensitive to minimum ionizing particles. A 1.5 kg chamber of superheated CF_3I has been operated for a total exposure of 250 kg-days. The presence of fluorine and iodine in the target makes COUPP sensitive to both SD and SI WIMP-nucleon couplings. The production of bubbles is monitored optically and via sound emission, reaching a reconstructed 3D spatial resolution of ~ 1 mm. It allows to reject boundary-events and to identify multiple neutron interactions. The most recent COUPP results set the most sensitive limit on SD WIMP-proton cross sections for a WIMP mass below 30 GeV. As an example, the upper bound on the SD coupling is 2.7×10^{-1} pb at a WIMP mass of 40 GeV.

In Fig. 8 we show the current CDMS and XENON10 upper bounds for the SI cross section

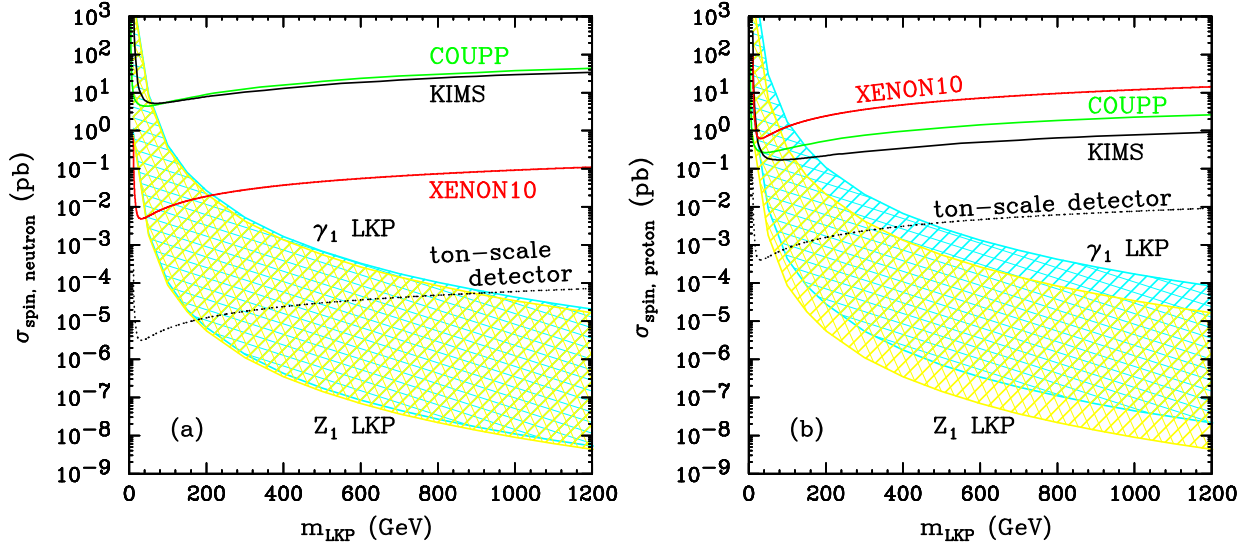


FIG. 9: Current experimental limits on the SD (a) neutron- and (b) proton-scattering cross section together with the predicted SD LKP-neutron (proton) cross sections for γ_1 (blue shaded) and Z_1 (yellow shaded). The solid curves for each plot are the upper bounds (90% C.L.) from the COUPP (green), KIMS (black) and XENON10 (red) experiments. The dotted line shows the expected sensitivity for a ton-scale detector which is obtained from Fig. 8 by a proper rescaling considering a Xenon detector. The γ_1 and Z_1 LKP areas are drawn with the same Δ_{q_1} convention as shown in Fig. 8.

together with projected sensitivities for SuperCDMS 25 kg, XENON100 and for a ton-scale detector. The LKP boundaries for γ_1 , Z_1 and γ_H as dark matter candidates are also shown, for a wide range of mass splittings ($0.01 < \Delta_{q_1} < 0.5$) and a fixed Higgs mass m_h of 120 GeV. The small mass splitting regions are excluded up to a mass of about 600 GeV, 900 GeV and 700 GeV for γ_1 , Z_1 and γ_H , respectively. For large mass splittings of $\Delta_{q_1} = 0.5$, only masses below about 100 GeV can be probed. Future ton-scale direct detection experiments should cover most of the interesting LKP parameter space.

In Fig. 9, we show the SD cross section limits for both (a) pure neutron and (b) pure proton couplings for three experiments together with the theoretical predictions for γ_1 and Z_1 for a range of mass splittings ($0.01 < \Delta_{q_1} < 0.5$). The most stringent SD pure neutron upper bound is set by the XENON10 experiment, while the best SD cross section for pure proton couplings in the region of interesting LKP masses (> 500 GeV) comes from the KIMS experiment. As explained in the previous section, the theoretical γ_1 and Z_1 regions are overlapping for pure neutron couplings, while for pure proton coupling these can be distinguished for a given mass splitting Δ_{q_1} .

In the following section we investigate the details of the LKP specific parameter spaces.

IV. LIMITS ON KALUZA-KLEIN DARK MATTER

In the previous sections we introduced the different dark matter candidates in UED models: KK gauge bosons (γ_1 and Z_1) and KK scalars (γ_H and H_1). On the theoretical side, we discussed the calculation of their relic densities and elastic scattering cross sections. On the experimental side, we described the different types of experiments which are sensitive to KK dark matter. We shall now combine our theoretical predictions with the current/future measurements discussed earlier. Where applicable, we shall also include constraints from high energy collider experiments. We shall be particularly interested in the region of small mass splittings Δ_{q_1} , which is problematic for collider searches, but promising for direct detection. We will concentrate on KK gauge boson dark matter (both γ_1 and Z_1), whose relic density can be reliably calculated, including all relevant coannihilation processes [23, 24].¹³

In Fig. 10 we present a combination of results for the case of (a) γ_1 and (b) Z_1 LKP in 5D UED. As we emphasized earlier, the two most relevant parameters are the LKP mass (m_{γ_1} or m_{Z_1} , correspondingly) and the mass splitting Δ_{q_1} between the LKP and the KK quarks. We therefore take both of these parameters as free and do not assume the MUED relation among them. For simplicity, we assume that the $SU(2)_W$ -doublet KK quarks and the $SU(2)_W$ -singlet KK quarks are degenerate, so that there is a single mass splitting parameter which we have been calling Δ_{q_1} . However, this assumption is only made for convenience, and does not represent a fundamental limitation – all of our results can be readily generalized for different KK quark mass splittings (i.e. several individual Δ parameters). The masses of the remaining KK particles in the spectrum are fixed as in Fig. 1: in the case of γ_1 LKP, we use the MUED spectrum, while in the case of Z_1 LKP, we take the gluon and the remaining particles to be respectively 20% and 10% heavier than the Z_1 . This choice is only made for definiteness, and does not carry a big impact on the validity of our results, as long as the remaining particles are sufficiently heavy so that they do not participate in coannihilation processes.

In the so defined parameter plane, in Fig. 10 we superimpose the limit on the spin-independent elastic scattering cross section, the limit on the relic abundance and the LHC reach in the four leptons plus missing energy ($4\ell + \cancel{E}_T$) channel which has been studied in [45].

¹³ The scalar candidates (γ_H and H_1) do not have spin-dependent interactions anyway, while their spin-independent scattering rates are similar to the examples we consider, as discussed in Sec. II C.

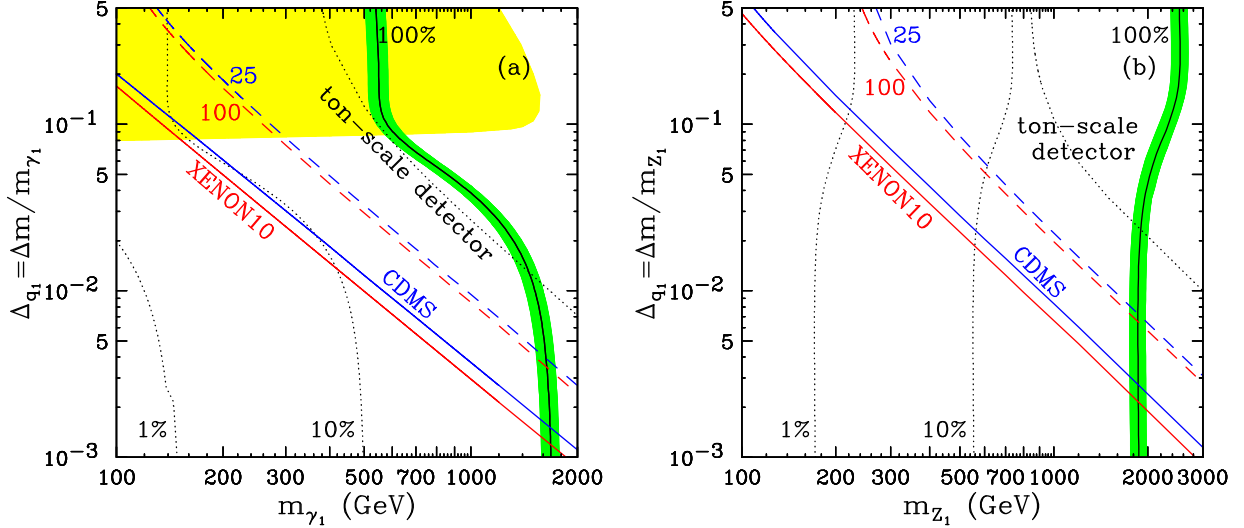


FIG. 10: Combined plot of the direct detection limit on the spin-independent cross section, the limit from the relic abundance and the LHC reach for (a) γ_1 and (b) Z_1 , in the parameter plane of the LKP mass and the mass splitting Δ_{q_1} . The remaining KK masses have been fixed as in Fig. 1 and the SM Higgs mass is $m_h = 120$ GeV. The black solid line accounts for all of the dark matter (100%) and the two black dotted lines show 10% and 1%, respectively. The green band shows the WMAP range, $0.1037 < \Omega_{CDM} h^2 < 0.1161$. The blue (red) solid line labelled by CDMS (XENON10) shows the current limit of the experiment whereas the dashed and dotted lines represent projected limits of future experiments as shown in Fig. 8. In the case of γ_1 LKP, a ton-scale experiment will rule out most of the parameter space while there is little parameter space left in the case of Z_1 LKP. The yellow region in the case of γ_1 LKP shows parameter space that could be covered by the collider search in the $4\ell + E_T$ channel at the LHC with a luminosity of 100 fb^{-1} [45].

This signature results from the pair production (direct or indirect) of $SU(2)_W$ -doublet KK quarks, which subsequently decay to Z_1 's and jets. The leptons (electrons or muons) arise from the $Z_1 \rightarrow \ell^+ \ell^- \gamma_1$ decay, whose branching fraction is approximately 1/3 [45]. Requiring a 5σ excess at a luminosity of 100 fb^{-1} , the LHC reach extends up to $R^{-1} \approx m_{\gamma_1} \sim 1.5 \text{ TeV}$, which is shown as the right-most boundary of the (yellow) shaded region in Fig. 10a. The slope of that boundary is due to the fact that as Δ_{q_1} increases, so do the KK quark masses, and their production cross sections are correspondingly getting suppressed, diminishing the reach. We account for the loss in cross section according to the results from Ref. [75], assuming also that, as expected, the level-2 KK particles are about two times heavier than those at level 1. Points which are well inside the (yellow) shaded region, of course, would be discovered much earlier at the LHC. Notice, however, that the LHC reach in this channel completely disappears for Δ_{q_1} less than about 8%. This is where the KK quarks become

lighter than the Z_1 (recall that in Fig. 10a m_{Z_1} was fixed according to the MUED spectrum) and the $q_1 \rightarrow Z_1$ decays are turned off. Instead, the KK quarks all decay directly to the γ_1 LKP and (relatively soft) jets, presenting a monumental challenge for an LHC discovery. So far there have been no studies of the collider phenomenology of a Z_1 LKP scenario, but it appears to be extremely challenging, especially if the KK quarks are light and decay directly to the LKP. This is why there is no LHC reach shown in Fig. 10b. In conclusion of our discussion of the collider reaches exhibited in Fig. 10, we draw attention once again to the lack of sensitivity at small Δ_{q_1} : such small mass splittings are quite problematic for collider searches (see, for example, [76, 77] for an analogous situation in supersymmetry).

In Fig. 10 we contrast the LHC reach with the relic density constraints and with the sensitivity of direct detection experiments. To this end we convert our results from Figs. 1 and 8 into the m_{LKP} - Δ_{q_1} plane shown in Fig. 10. The green shaded region labelled by 100% represents 2σ WMAP band, $0.1037 < \Omega_{CDM}h^2 < 0.1161$ [58] and the black solid line inside this band is the central value $\Omega_{CDM}h^2 = 0.1099$. The region above and to the right of this band is ruled out since UED would then predict too much dark matter. The green-shaded region is where KK dark matter is sufficient to explain all of the dark matter in the universe, while in the remaining region to the left of the green band the LKP can make up only a fraction of the dark matter in the universe. We have indicated with the black dotted contours the parameter region where the LKP would contribute only 10% and 1% to the total dark matter budget. Finally, the solid (CDMS in blue and XENON10 in red) lines show the current direct detection limits, while the dotted and dashed lines show projected sensitivities for future experiments (for details, refer back to Sec. III)¹⁴.

Fig. 10 demonstrates the complementarity between the three different types of probes which we are considering. First, the parameter space region at very large m_{LKP} is inconsistent with cosmology – if the dark matter WIMP is too heavy, its relic density is too large. The exact numerical bound on the LKP mass may vary, depending on the particle nature of the WIMP (compare Fig. 10a to Fig. 10b) and the presence or absence of coannihilations (compare the m_{LKP} bound at small Δ_{q_1} to the bound at large Δ_{q_1}). Nevertheless, we can

¹⁴ Here and in the rest of the paper, when presenting experimental limits in an underdense or an overdense parameter space region, we do not rescale the expected direct detection rates with the calculated relic density. The latter is much more model-dependent, e.g. the mismatch with the WMAP value may be fixed by non-standard cosmological evolution, having no effect on the rest of our analysis.

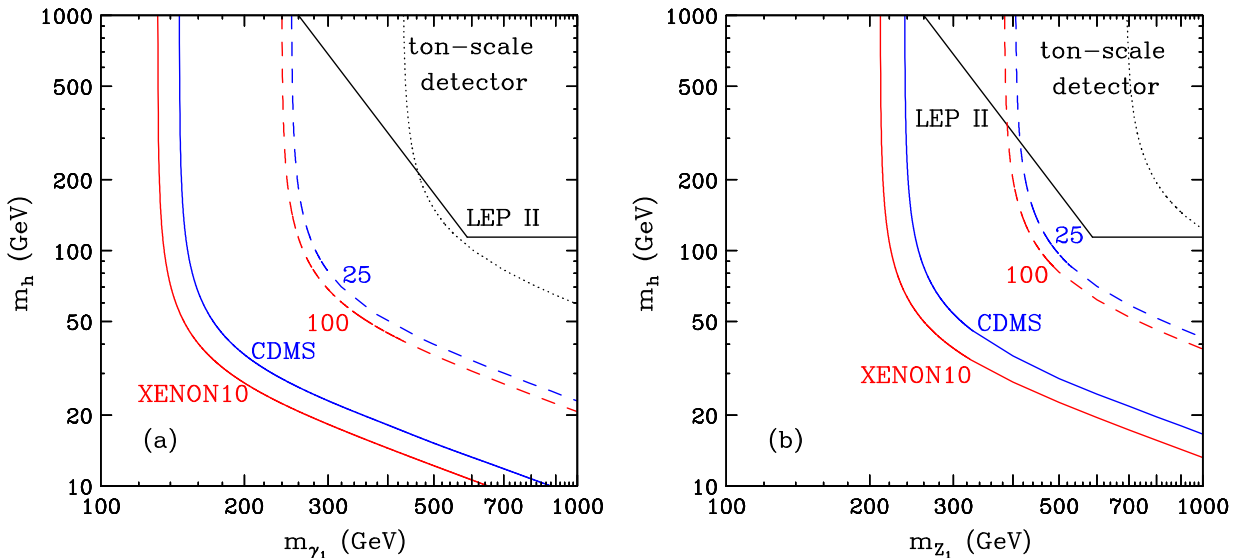


FIG. 11: Limit on the SM Higgs mass m_h and the LKP mass for (a) γ_1 and (b) Z_1 for a given $\Delta_{q_1} = 0.1$. The horizontal black solid line is the lower bound on m_h from LEP-II (90% C.L. at top quark mass 173 GeV). The diagonal black solid line delineates the region disfavored by precision data. The solid curves are the current (90% C.L.) limits from CDMS (in blue) and XENON10 (in red). The dashed curves (SuperCDMS 25 kg and XENON100) and dotted line (ton-scale detector) are the projected sensitivities for the future experiments.

see that, in general, cosmology does provide an upper limit on the WIMP mass. On the other hand, colliders are sensitive to the region of relatively large mass splittings Δ_{q_1} , while direct detection experiments are at their best at small Δ_{q_1} and small m_{LKP} . The relevant parameter space is therefore getting squeezed from opposite directions and is bound to be covered eventually. This is already seen in the case of γ_1 LKP from Fig. 10a: the future experiments push up the current limit almost to the WMAP band. Unfortunately in the case of Z_1 LKP the available parameter space is larger and will not be closed with the currently envisioned experiments alone. However, one should keep in mind that detailed LHC studies for that scenario are still lacking.

While previously we already argued that m_{LKP} and Δ_{q_1} are the most relevant parameters for UED dark matter phenomenology, for completeness we also investigate the dependence on the SM Higgs mass m_h , which is currently still unknown. In Fig. 11 we therefore translate the information from Fig. 8 into the m_{LKP} - m_h plane, for a given fixed KK mass splitting $\Delta = 0.1$ now taking the Higgs mass m_h as a free parameter. In each panel, the horizontal black solid lines mark the current Higgs mass bound of 114 GeV while the diagonal black solid lines show

the indirect limit from the oblique corrections in this model [59].¹⁵ For low m_h , the limit on the LKP mass (or equivalently, the compactification scale) is $m_{LKP} \sim R^{-1} \gtrsim 600 \text{ GeV}$ (for $m_t = 173 \text{ GeV}$), but it gets weaker for larger m_h , so that m_{LKP} values as low as 300 GeV are still allowed if the SM Higgs boson is very heavy [60]. In Fig. 11 we also show the current (solid lines) limits from CDMS (in blue) and XENON10 (in red), their projected near-future sensitivities, SuperCDMS 25 kg and XENON100 (dashed lines), and the projected sensitivity of a ton-scale detector (dotted line). The shape of these contours is easy to understand. At large m_h , the Higgs exchange diagram in Fig. 4 decouples, the elastic scattering rate becomes independent of m_h and the direct detection experimental sensitivity is only a function of m_{LKP} (since Δ_{q_1} is held fixed). In the other extreme, at small m_h , the Higgs exchange diagram dominates, and the sensitivity now depends on both m_h and m_{LKP} . Unfortunately, for $\Delta = 0.1$ the current direct detection bounds do not extend into the interesting parameter space region, but future experiments will eventually start probing the large m_h corner of the allowed parameter space. On the positive side, one important lesson from Fig. 11 is that the m_h dependence starts showing up only at very low values of m_h , which have already been ruled out by the Higgs searches at colliders. This observation confirms that when it comes to interpreting existing and future experimental limits on WIMPs in terms of model parameters, m_{LKP} and Δ_{q_1} are indeed the primary parameters, while m_h plays a rather secondary role.

We remind the reader that the LHC will be able to probe all of the parameter space shown in Fig. 11a through the $4\ell + \cancel{E}_T$ signature, while the discovery of UED in Fig. 11b appears quite problematic. Of course, the SM Higgs boson will be discovered in both cases, for the full range of m_h masses shown.

We now turn to a discussion of the corresponding spin-dependent elastic scattering cross sections, which also exhibit an enhancement at small Δ_{q_1} , as shown in Fig. 6. Similar to Fig. 10, in Fig. 12 we combine existing limits from three different experiments (XENON10, KIMS and COUPP) in the m_{LKP} - Δ_{q_1} plane. Panel (a) (panel (b)) shows the constraints from the WIMP-neutron (WIMP-proton) SD cross sections. The rest of the KK spectrum

¹⁵ One should keep in mind that the latter have been calculated only for the case of γ_1 LKP, and only within the framework of minimal UED. The line shown in Fig. 11b is therefore only for illustration. Furthermore, the γ_1 calculation itself may be subject to modifications in the more general scenarios which we are considering here.

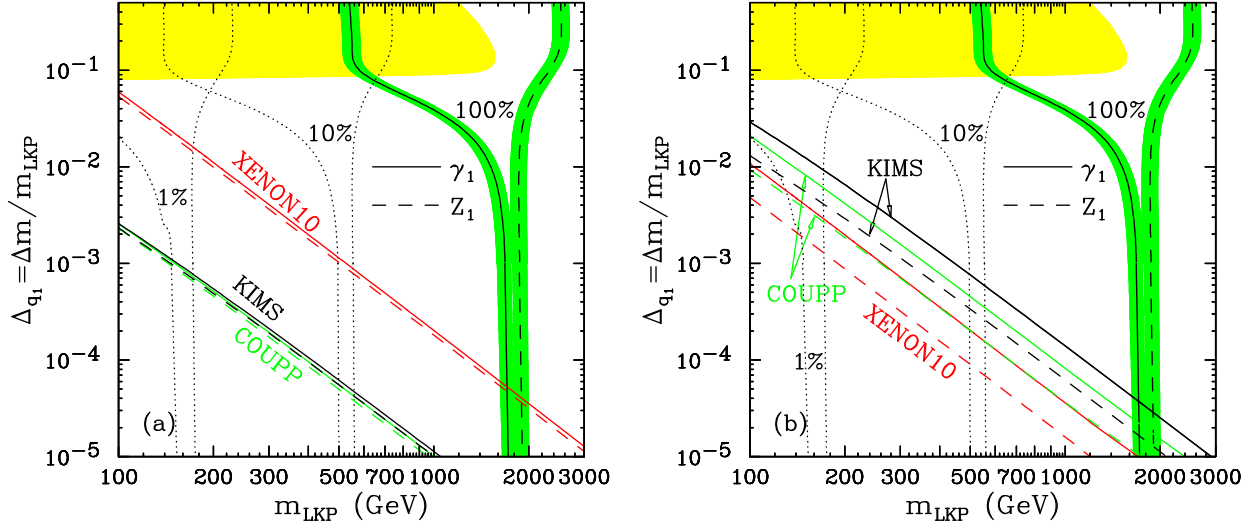


FIG. 12: Experimental upper bounds (90% C.L.) on the spin-dependent elastic scattering cross sections on (a) neutrons and (b) protons in the m_{LKP} - Δ_{q_1} plane. The solid (dashed) curves are limits on γ_1 (Z_1) for each experiment. Shaded regions and dotted lines are defined in the same way as in Fig. 10. The depicted LHC reach (yellow shaded region) applies only to the case of γ_1 LKP.

has been fixed as in Figs. 1 and 10, and $m_h = 120$ GeV. The solid (dashed) curves are limits on γ_1 (Z_1) for each experiment. The constraints from LHC and WMAP on the m_{LKP} - Δ_{q_1} parameter space are the same as in Fig. 10.

By comparing Figs. 10 and 12 we see that, as expected, the parameter space constraints from SI interactions are stronger than those from SD interactions. For example, in perhaps the most interesting range of LKP masses from 300 GeV to 1 TeV, the SI limits on Δ_{q_1} in Fig. 10 range from a few times 10^{-2} down to a few times 10^{-3} . On the other hand, the SD bounds on Δ_{q_1} for the same range of m_{LKP} are about an order of magnitude smaller (i.e. weaker). We also notice that the constraints for γ_1 LKP are stronger than for Z_1 LKP. This can be easily understood by comparing Fig. 6a and Fig. 6b: for the same LKP mass and KK mass splitting, the γ_1 SD cross sections are typically larger.

Fig. 12 also reveals that the experiments rank differently with respect to their SD limits on protons and neutrons. For example, KIMS and COUPP are more sensitive to the proton cross section, while XENON10 is more sensitive to the neutron cross section. As a result, the current best SD limit on protons comes from KIMS, but the current best SD limit on neutrons comes from XENON10. Combining all experimental results can give a very good constraint on the a_p - a_n parameter space. Fig. 13a (Fig. 13b) shows combined results for $m_{LKP} = 50$ GeV ($m_{LKP} = 500$ GeV) in the (model-independent) a_p - a_n parameter space.

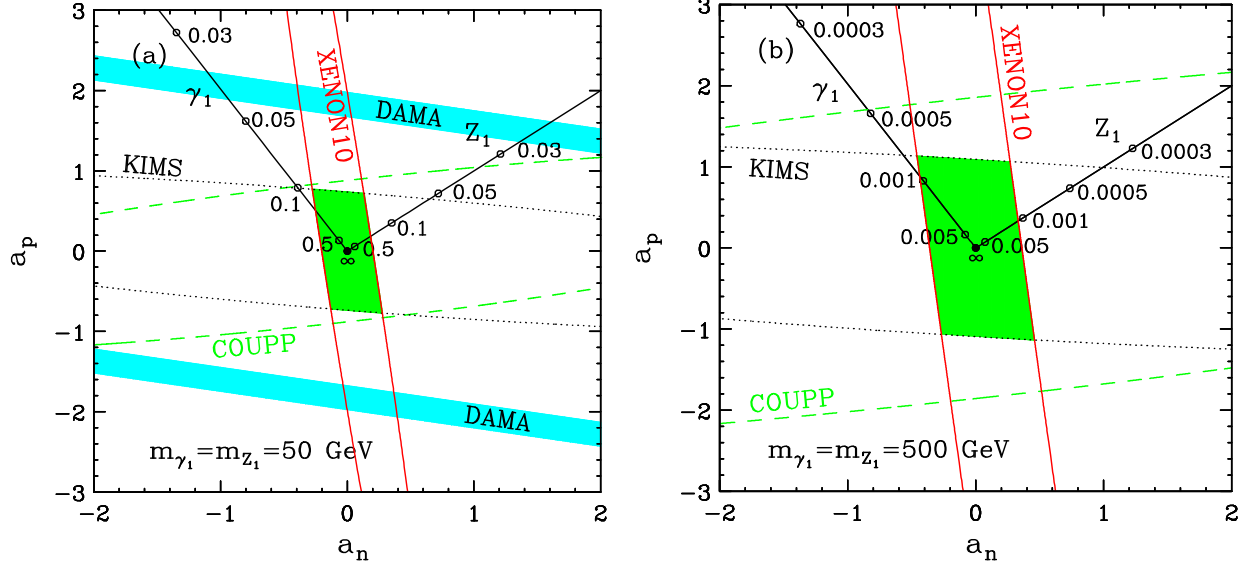


FIG. 13: Experimental limits on the a_p - a_n parameter space for (a) $m_{LKP} = 50$ GeV and (b) $m_{LKP} = 500$ GeV. The contours show limits from XENON10 (red solid line), KIMS (black dotted line) and COUPP (green dashed line). The blue near-horizontal bands show the evidence regions allowed by DAMA [78], while the green region shows the parameter space allowed by all current experimental results. The two straight lines originating from $a_n = a_p = 0$ are the theoretical predictions for a_p and a_n in the case of γ_1 or Z_1 LKP in 5D UED. These theory lines are parametrized by the value of Δ_{q_1} as indicated by a few representative points.

The contours show limits from XENON10 (red solid line), KIMS (black dotted line) and COUPP (green dashed line). The blue near-horizontal bands show the evidence regions allowed by DAMA [78], while the green region shows the parameter space allowed by all current experiments. Note that these limits were computed in two different ways. The results from KIMS and COUPP are based on the method proposed in [63] whereas those from DAMA and XENON10 are calculated as advocated in [78]. We believe that the latter is more accurate since limits are computed for all angles in the a_p - a_n plane separately whereas the former solely relies on the limits calculated considering pure coupling to neutrons and protons respectively. More details about these calculations can be found in the appendix. The two straight lines originating from $a_n = a_p = 0$ are the theoretical predictions for a_p and a_n in the case of γ_1 or Z_1 LKP in 5D UED. These theory lines are parametrized by the value of Δ_{q_1} as indicated by a few representative points. The feature which is readily apparent in Fig. 13 is the orthogonality between the regions allowed by the a_p -sensitive experiments like KIMS and COUPP, on the one side, and the a_n -sensitive experiments like XENON10, on the other. This indicates the complementarity of the two groups of experiments: the

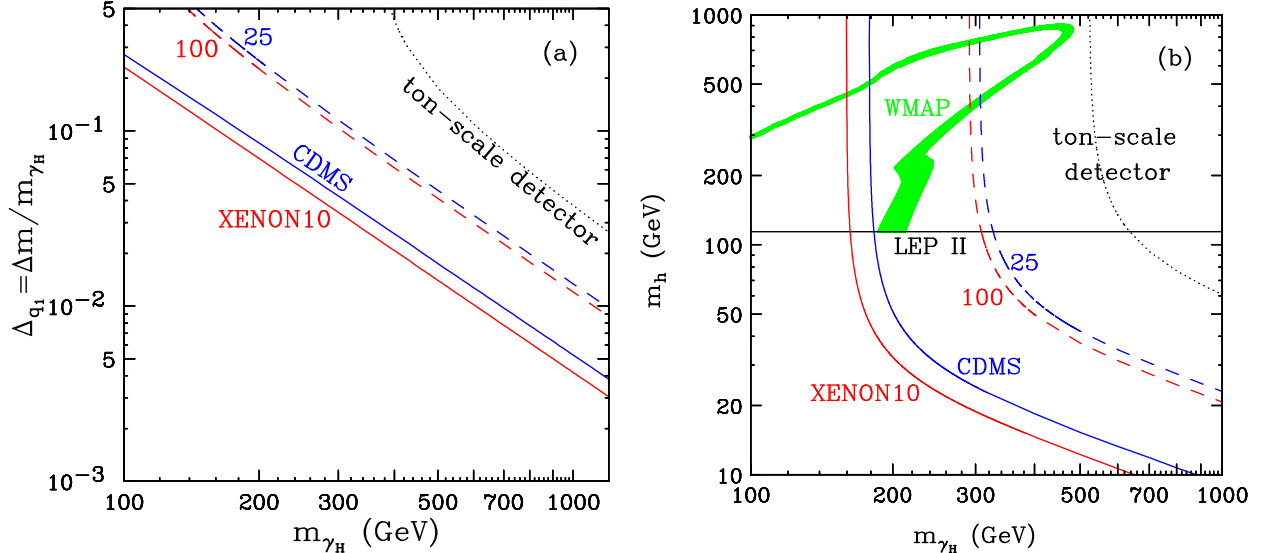


FIG. 14: Experimental limits (90% C.L.) on the scalar LKP (γ_H) in 6D UED. (a) Lower bound of Δ_{q1} vs m_{γ_H} for $m_h = 120$ GeV. The solid lines are the current experimental lower bounds on Δ_{q1} for a given m_{γ_H} from CDMS (blue) and XENON10 (red). SuperCDMS 25 kg and XENON100 projected sensitivities are drawn with dashed lines. The dotted line shows the projected sensitivity of a ton-scale experiment. (b) Lower bound of the Higgs mass (m_h) as a function of m_{γ_H} for a fixed $\Delta_{q1} = 0.1$. The WMAP allowed range is the green shaded region. The LEP II lower bound on m_h is shown as the black solid line.

green-shaded region allowed by the combination of all experiments is substantially more narrow than the region allowed by each individual experiment.

In conclusion of this section, we shall also consider KK dark matter candidates in models with two universal extra dimensions (6D UED). As mentioned in Sec. II A the novel possibility here compared to 5D UED is the scalar photon (γ_H) LKP. As a spin zero particle, it has no spin-dependent interactions and can only be detected through its spin-independent elastic scattering. Fig. 14a (Fig. 14b) is the analogue of Fig. 10 (Fig. 11) for the case of γ_H LKP. In Fig. 14a we show lower bounds on Δ_{q1} versus the mass m_{γ_H} of the scalar photon, for a fixed Higgs mass ($m_h = 120$ GeV). The solid lines indicate the current experimental limits from CDMS (blue) and XENON10 (red). The dashed lines are the projected sensitivities of SuperCDMS 25 kg and XENON100 and the dotted line is the projected sensitivity of a ton-scale detector. Since the cosmologically preferred mass range for γ_H is much lower (~ 200 GeV before accounting for coannihilations) than for the LKP in 5D UED, the constraints are quite powerful – in particular, the future ton-scale experiments are expected to cover most of the interesting mass splitting (Δ_{q1}) region.

In Fig. 14b we show lower bounds of the Higgs mass m_h as a function of m_{γ_H} for a fixed $\Delta_{q_1} = 0.1$. The WMAP preferred parameter space is marked as the green shaded region, while the black solid line is the LEP II lower limit on m_h . The contours resemble in shape those seen earlier in Fig. 11. In particular, we notice that within the LEP II allowed range, the Higgs mass does not have a large impact on the direct detection bounds. However, if the LHC finds a SM Higgs boson with a mass smaller than ~ 300 GeV, then the WMAP bound would constrain the mass of γ_H within a relatively narrow mass ranges at a given mass splitting (Δ_{q_1}). For example in Fig. 14b, where the fixed mass splitting is $\Delta_{q_1} = 0.1$, the corresponding constraint on the mass of γ_H would be $180 \text{ GeV} < m_{\gamma_H} < 250 \text{ GeV}$. In fact, this conclusion is rather insensitive to the particular choice of Δ_{q_1} . This is due to the fact that γ_H self-annihilation is helicity-suppressed and gauge boson final states are dominant in the WMAP allowed regions. Therefore, Fig. 14b would look qualitatively similar, if a different value of Δ_{q_1} were used.

V. CONCLUSIONS

The dark matter puzzle is among the most intriguing questions in particle physics. Its origin resides in cosmological observations such as the rotation curves of galaxies, cosmic microwave background, gravitational lensing, large scale structure, the mass to luminosity ratio and so on. Interestingly, many scenarios of new physics beyond the Standard Model provide a stable neutral particle which, in principle, can be produced and observed at colliders. In fact, one of the primary motivations for SUSY has always been the fact that it naturally accommodates a WIMP candidate. More recently, we have learned that extra dimensional models provide a viable alternative to SUSY dark matter, namely KK dark matter. Both of these scenarios have been attracting a lot of attention in terms of collider and astrophysical aspects. In this paper we performed a comprehensive phenomenological analysis of KK dark matter in universal extra dimensions, extending previous studies by considering new LKP candidates (Z_1 and H_1). We also revisited the cases of γ_1 and γ_H LKP, focusing on the possibility of a small mass splitting with the KK quarks. All of these features can be realized in non-minimal UED scenarios and therefore deserve attention.

In our analysis we included the relevant theoretical constraints from cosmology (the relic density of KK dark matter) and particle physics (low energy precision data). We accounted

for all coannihilation processes in our relic density calculation, focusing on coannihilations with KK quarks since they play an important role for direct detection at small mass splittings.

We then contrasted the sensitivities of the LHC and the different types of direct detection experiments, and exhibited their complementarity. We demonstrated that the $m_{LKP} - \Delta_{q_1}$ parameter space is both convenient and sufficient for a simultaneous discussion of collider and direct detection searches. Collider experiments like the LHC and possibly ILC are sensitive to the region of relatively low m_{LKP} and sufficiently large Δ_{q_1} . On the other hand, direct detection experiments do best at relatively low m_{LKP} and small Δ_{q_1} . Finally, cosmology rules out the region of very large m_{LKP} . We see that, at least in principle, the combination of all three types of constraints has the potential to completely cover the relevant parameter space. We showed that with the expected sensitivity of the next generation direct detection experiments, the coverage is almost complete in the case of γ_1 LKP.

In conclusion, we summarize the main lessons from each of the three main areas in our study, and point towards interesting directions for future work.

- *Direct detection of KK dark matter.* The direct detection prospects are greatly enhanced when the LKP becomes degenerate with the KK quarks [26]. Therefore, the mass splitting Δ_{q_1} is a key parameter which is worth exploiting by the experimental collaborations in presenting their limits. The conventional approach is to overlay the results of random scans over the full parameter space of a given model over the model-independent exclusion curves from Figs. 8 and 9. There are several problems with this. First, due to the multitude of parameters being scanned, such scans are not sufficiently exhaustive and are almost guaranteed to miss the relevant parts of parameter space. For example, suppose we scan a KK quark mass in the range from m_{LKP} up to some maximum value $m_{q_1}^{max}$. In order to obtain a *single* parameter space point at a given Δ_{q_1} , the number of points sampled along the m_{q_1} direction should be at least

$$N = \frac{m_{q_1}^{max} - m_{LKP}}{m_{q_1} - m_{LKP}} = \frac{m_{q_1}^{max} - m_{LKP}}{m_{LKP}} \frac{1}{\Delta_{q_1}} \sim \frac{1}{\Delta_{q_1}} .$$

In order to probe mass degeneracies of $\Delta_{q_1} \sim 0.01$, one should therefore generate at least 10^2 points *along each parameter dimension*. It is then clear that random scans cannot effectively probe models which have more than a few input parameters. For

example, typical SUSY scans often utilize a constrained parameter space which nevertheless still has on the order of 10-15 parameters. In that case, seeing the effects of 1% degeneracies would require $10^{20} - 10^{30}$ total points – a number which is obviously impractical. Furthermore, many of the scanned parameters often have little effect on the experimental signals being discussed. We therefore find it much more efficient and illuminating to forego such general scans in favor of simple parametrizations which would contain only the variables relevant for the experimental search. A simple implementation of this idea is the $m_{LKP} - \Delta_{q_1}$ parameter space used in Figs. 10 and 12. Notice that our argument is not limited to UED models – the mass of the dark matter particle and the mass splitting are expected to be the two most important parameters for dark matter searches in any other theory (such as SUSY, little Higgs, warped extra dimensions, etc.).

- *Collider searches for KK dark matter.* While beneficial for direct DM detection, mass degeneracies are generally problematic for collider searches, since they degrade the quality of the discovery signatures. For example, at small Δ_{q_1} the KK quark decay products become softer, and the leptonic modes may altogether turn off. Detailed LHC studies for these challenging situations are still lacking and are definitely worth undertaking. In particular, the LHC phenomenology of Z_1 or H_1 LKP has never been discussed.
- *Theoretical calculations related to KK dark matter.* In this paper we have reviewed the main ingredients of a complete analysis of KK dark matter phenomenology. We emphasized the importance of including the effect of coannihilations in the case of small mass splittings which are relevant for experimental searches. However, there are still several missing pieces which are needed to improve the accuracy of our predictions. While the relic density calculation for γ_1 and Z_1 LKP is on a relatively firm footing, since the corresponding coannihilation processes are known, the complete calculation of coannihilation effects in case of H_1 , γ_H or Z_H LKP is still lacking. Similarly, one would like to have available the precise calculation of the heavy flavor contribution to the LKP elastic scattering cross section on nucleons. We are hoping that it would take less than a WIMP direct detection signal to jumpstart the theoretical efforts in this direction.

Acknowledgments

We would like to thank CDMS collaboration, COUPP collaboration, KIMS collaboration and XENON10 collaboration for providing important information, and Tim Tait for useful discussion. SA and LB are supported by the Swiss National Foundation SNF Grant No 20-118119 and by the Volkswagen Foundation. KM is supported in part by a US Department of Energy Outstanding Junior Investigator award under grant DE-FG02-97ER41029. Fermilab is operated by Fermi Research Alliance, LLC under Contract No. DE-AC02-07CH11359 with the U.S. Department of Energy.

VI. APPENDIX: EVENT RATE CALCULATIONS FOR DIRECT DETECTION EXPERIMENTS

Given the interaction cross section of LKPs with nucleons the expected event rates for each experiment can be calculated. A spherical halo model is conventionally used for a consistent comparison of the different experimental results. Spin-independent (spin-dependent) interactions with non-zero momentum transfer to the nucleus demand nuclear (spin) form factor corrections in the cross section calculations. Furthermore it is a common procedure to normalize the cross sections to the scattering from a single nucleon. In the following we describe the details of our event rate calculations for direct detection experiments particularly with regard to setting limits on the cross sections and couplings. Further information can be found in reference [67].

A. Spherical halo model and differential event rates

The dark matter halo is assumed to be an isothermal and isotropic sphere of an ideal WIMP gas obeying a Maxwell-Boltzmann velocity distribution

$$f(\vec{v}, \vec{v}_E) \sim e^{-\frac{(\vec{v} + \vec{v}_E)^2}{v_0^2}}, \quad (28)$$

where \vec{v} denotes the velocity of the WIMPs in the rest frame of the earth and \vec{v}_E the velocity of the earth with respect to the motionless galactic halo. v_0 ($= 220$ km/s) is the characteristic velocity of the distribution which is assumed to be equal to the galactic rotation velocity

v_r . There are three contributions to \vec{v}_E : the galactic rotation velocity \vec{v}_r , the velocity of the sun with respect to the galactic disc \vec{v}_s and the velocity of the earth around the sun \vec{v}_{orb} . Its main contribution is given by

$$v_E(t) = v_r + v_s + v_{orb} \cos \beta \cos \left(2\pi \frac{t - t_0}{T} \right), \quad (29)$$

taking the angle $\beta = 59.575^\circ$ between the earth orbital plane and the galactic plane into account. The velocities are given by $v_r = 220$ km/s, $v_s = 12$ km/s and $v_{orb} = 29.79$ km/s respectively. t_0 is the day in a year corresponding to the 2nd June ($t_0 = 152.5$) and T is the number of days in a year ($T = 365.25$). The modulation of the mean velocity is about $\pm 6.5\%$. Since we are not investigating time depending properties of event rates such as annual modulation effects, we use the mean velocity of the earth $\langle v_E \rangle = 232$ km/s, averaged over one year. The velocity distribution of WIMPs is isotropic in the galactic rest frame. It is limited by the escape velocity of the WIMPs (v_{esc}) from the galactic halo

$$|\vec{v} + \vec{v}_E| < v_{esc}, \quad (30)$$

which yields a maximum WIMP velocity

$$v_{max}(\theta, t) = \sqrt{v_{esc}^2 - v_E^2(t)(1 - \cos^2 \theta)} - v_E(t) \cos \theta, \quad (31)$$

with θ being the scattering angle in the galactic rest frame. In our calculations we take $v_{esc} = 544$ km/s [64]. We obtain a mean maximum WIMP velocity given by $\langle v_{max} \rangle = 518.3$ km/s by averaging over a year and the scattering angle. The maximum recoil energy $E_{R_{max}}$ of the nucleus is given by

$$E_{R_{max}} = \frac{1}{2} m_{LKP} v_{max}^2 r, \quad (32)$$

with the kinematic factor

$$r = \frac{4m_{LKP}m_T}{(m_{LKP} + m_T)^2}. \quad (33)$$

The differential event rate is

$$\frac{dR}{dE_R} = \frac{R_0(\sigma)}{E_0 r} \frac{k_0}{k_1} \left[\frac{\sqrt{\pi}}{4} \frac{v_0}{\langle v_E \rangle} \left[\operatorname{erf} \left(\frac{v_{min} + \langle v_E \rangle}{v_0} \right) - \operatorname{erf} \left(\frac{v_{min} - \langle v_E \rangle}{v_0} \right) \right] - e^{-\frac{v_{esc}^2}{v_0^2}} \right]. \quad (34)$$

$R_0(\sigma)$ is the total event rate for a given cross section assuming $v_E = 0$, $v_{esc} = \infty$ and integrated over recoil energies from $E_R = 0$ to $E_R = \infty$. v_{min} is defined as the minimum velocity leading to a certain recoil energy E_R whereas E_0 denotes the energy carried by a WIMP with the velocity v_0 . The ratio k_0/k_1 arises from the normalization of the WIMP density distribution. For completeness all relevant formulas are given below:

$$R_0(\sigma) = \frac{2}{\sqrt{\pi}} \frac{N_0}{A_u} \frac{\rho}{m_{LKP}} \sigma v_0, \quad (35)$$

$$v_{min} = \sqrt{\frac{E_R}{E_0 r}} v_0, \quad (36)$$

$$E_0 = \frac{1}{2} m_{LKP} v_0^2, \quad (37)$$

$$\frac{k_0}{k_1} = \left[\operatorname{erf} \left(\frac{v_{esc}}{v_0} \right) - \frac{2}{\sqrt{\pi}} \frac{v_{esc}}{v_0} e^{-\frac{v_{esc}^2}{v_0^2}} \right]^{-1}. \quad (38)$$

N_0 is the Avogadro constant and A_u is the atomic mass unit. The local dark matter density $\rho = 0.3 \text{ GeV/cm}^3$ is taken from [65]. σ denotes either the spin-independent or spin-dependent cross section which for the case of γ_1 LKP are given in (15) and (23) respectively.

B. Expected event rate: spin-independent interactions

The spin-independent cross-section given in equation (15) normalized to a single nucleon can be written as

$$\sigma_{scalar}^{p,n} = \frac{1}{A^2} \frac{\mu_{p,n}^2}{\mu^2} \sigma_{scalar}. \quad (39)$$

Owing to the finite size of the target nucleus, the LKP-nucleus cross section is valid only for the case of zero-momentum transfer ($q = 0$). For non-zero momentum transfer, a form factor correction needs to be considered:

$$\sigma_{SI} = \sigma_{scalar} F_{SI}^2, \quad (40)$$

where F_{SI} is the nuclear form factor. We used Helm's model [79] :

$$F_{SI}(qr_n) = 3 \frac{j_1(qr_n)}{qr_n} e^{-\frac{(qr_n)^2}{2}}, \quad (41)$$

with the spherical Bessel function j_1 , the effective nuclear radius $r_n = \sqrt{c^2 + \frac{7}{3}\pi^2 a^2 - 5s^2}$ with $a = 0.52$ fm and $c = 1.23\sqrt[3]{A} - 0.60$ fm, and the nuclear skin thickness $s = 1$ fm [67].

The spin-independent differential event rate for finite-momentum transfer can then be obtained by replacing σ with σ_{SI} in (35) and thus in (34). If the WIMP target consists of more than one element, the respective abundances of each isotope f_i have to be considered. The total differential event rate for a specific WIMP target is

$$\frac{dR_{SI}}{dE_R} = \sum_i f_i \frac{dR_{SI}^i}{dE_R}. \quad (42)$$

The expected number of events for spin-independent interactions for a given experiment can then be written as

$$N_{SI} = \int_{q_{\min}}^{\min(q_{\max}, \langle E_{R_{\max}} \rangle)} dE_R \frac{dR_{SI}}{dE_R} \epsilon(E_R) MT, \quad (43)$$

where MT denotes the total detector exposure in kg-days and $\epsilon(E_R)$ the WIMP detection efficiency as a function of recoil energy. q_{\min} and q_{\max} denote the lower and upper bound of the WIMP-nucleus recoil energy which is considered in the data analysis. We truncated the integral at the minimum of the upper analysis limit and the averaged maximum recoil energy $\langle E_{R_{\max}} \rangle$. Due to its definition there is a fraction of WIMPs which can give rise to a higher maximum recoil energy especially those which hit the detector in a head-on collision. However since the differential event rates decrease approximately exponentially the actual value of this cut-off only effects the results for WIMPs with low masses (~ 10 GeV). We used the statistical method proposed in [80] to obtain the XENON10 limits.

C. Expected event rate: spin-dependent interactions

Given the spin-dependent cross section (23) and the differential event rate (34), the expected event rate calculation for axial-vector interactions is similar to the spin-independent case. We first normalize the cross section to the scattering from a single nucleon. The nucleon spin expectation values are $\langle S_p \rangle = \frac{1}{2}$ and $\langle S_n \rangle = 0$ and $\langle S_p \rangle = 0$ and $\langle S_n \rangle = \frac{1}{2}$, for a proton

and a neutron respectively. Using these values the SD cross section for a single nucleon is

$$\sigma_{\text{spin}}^{p,n} = \frac{24}{\pi} G_F^2 \mu_{p,n}^2 a_{p,n}^2. \quad (44)$$

Comparing (44) to (23), the SD cross section with proper normalization can be written as

$$\sigma_{\text{spin}}^{p,n} = \frac{3}{4} \frac{\mu_{p,n}^2}{\mu^2} \frac{J_N}{J_N + 1} \frac{1}{\langle S_{p,n} \rangle^2} \sigma_{\text{spin}}. \quad (45)$$

Similar to the SI case a SD form factor has to be introduced to account for non-zero momentum transfer

$$\sigma_{SD} = \sigma_{\text{spin}} F_{SD}^2, \quad (46)$$

where F_{SD}^2 can be written in the form [81]

$$F_{SD}^2(q) = \frac{S(q)}{S(0)}, \quad (47)$$

with the spin structure function $S(q)$. What makes the limit calculations in the SD case involved is the fact that $S(q)$ depends on the WIMP-nucleon couplings. For the spin-dependent limits for XENON10 we used the form factors obtained using the Bonn A potential given in [82]. In the zero-momentum transfer limit, the spin structure function $S(q)$ can be evaluated:

$$S(0) = \frac{2J_N + 1}{\pi} J_N (J_N + 1) \Lambda^2, \quad (48)$$

where Λ is defined as

$$\Lambda = \frac{a_p \langle S_p \rangle + a_n \langle S_n \rangle}{J_N}. \quad (49)$$

For finite momentum transfer it is a common procedure to translate the WIMP-proton and WIMP-neutron couplings a_p and a_n into isoscalar and isovector spin couplings a_0 and a_1 using

$$\begin{aligned} a_0 &= a_p + a_n \\ a_1 &= a_p - a_n, \end{aligned} \quad (50)$$

so that the spin structure function can be written as

$$S(q) = a_0^2 S_{00}(q) + a_1^2 S_{11}(q) + a_0 a_1 S_{01}(q). \quad (51)$$

S_{00} , S_{11} and S_{01} represent an isoscalar, isovector and interference term respectively. The shape of $S(q)$ is determined by the ratio $\frac{a_p}{a_n}$ while its magnitude is proportional to $a_p^2 + a_n^2$. Following [78] we consider polar coordinates in the (a_p, a_n) subspace:

$$\begin{aligned} a_p &= a \sin \theta \\ a_n &= a \cos \theta. \end{aligned} \quad (52)$$

Pure proton and neutron couplings are obtained by setting $\theta = 90^\circ$ and $\theta = 0^\circ$, respectively. Inserting this ansatz into (51) yields

$$S(q) = a^2 \left((\sin \theta + \cos \theta)^2 S_{00}(q) + (\sin \theta - \cos \theta)^2 S_{11}(q) - \cos(2\theta) S_{01}(q) \right). \quad (53)$$

Similar to (43) the number of events is obtained by evaluating the integral

$$N_{SD} = \sum_i f_i \int_{q_{\min}}^{\min(q_{\max}, \langle E_{R_{\max}} \rangle)} dE_R \frac{dR_{SD}^i}{dE_R} \epsilon(E_R) MT. \quad (54)$$

N_{SD} can be re-written in the form

$$N_{SD} = A a_p^2 + 2 B a_p a_n + C a_n^2, \quad (55)$$

with A , B and C being constant for a given WIMP mass. Inserting (52) yields

$$N_{SD} = a^2 \left(A \sin^2 \theta + 2 B \sin \theta \cos \theta + C \cos^2 \theta \right). \quad (56)$$

In order to calculate the limits on the WIMP-nucleon SD couplings, for any WIMP mass of interest we performed a scan over the angle θ from $0^\circ - 360^\circ$. Thus, as in the spin-independent case, a limit on a^2 can be set. Since (56) is a quadratic equation the limits are expected to be ellipses in the (a_p, a_n) subspace. The allowed (a_p, a_n) parameter space is

restricted to the inner region of these ellipses.

- [1] For a recent review, see G. Bertone, D. Hooper and J. Silk, “Particle dark matter: Evidence, candidates and constraints,” *Phys. Rept.* **405**, 279 (2005) [arXiv:hep-ph/0404175].
- [2] For a review, see G. Jungman, M. Kamionkowski and K. Griest, “Supersymmetric dark matter,” *Phys. Rept.* **267**, 195 (1996) [arXiv:hep-ph/9506380].
- [3] For a review, see D. Hooper and S. Profumo, “Dark matter and collider phenomenology of universal extra dimensions,” *Phys. Rept.* **453**, 29 (2007) [arXiv:hep-ph/0701197].
- [4] H. C. Cheng and I. Low, “TeV symmetry and the little hierarchy problem,” *JHEP* **0309**, 051 (2003) [arXiv:hep-ph/0308199].
- [5] A. Birkedal, A. Noble, M. Perelstein and A. Spray, “Little Higgs dark matter,” *Phys. Rev. D* **74**, 035002 (2006) [arXiv:hep-ph/0603077].
- [6] T. Hur, H. S. Lee and S. Nasri, “A Supersymmetric U(1)' Model with Multiple Dark Matters,” *Phys. Rev. D* **77**, 015008 (2008) [arXiv:0710.2653 [hep-ph]].
- [7] H. S. Lee, “Lightest U-parity Particle (LUP) dark matter,” *Phys. Lett. B* **663**, 255 (2008) [arXiv:0802.0506 [hep-ph]].
- [8] C. Arina and N. Fornengo, “Sneutrino cold dark matter, a new analysis: relic abundance and detection rates,” *JHEP* **0711**, 029 (2007) [arXiv:0709.4477 [hep-ph]].
- [9] H. S. Lee, K. T. Matchev and S. Nasri, “Revival of the thermal sneutrino dark matter,” *Phys. Rev. D* **76**, 041302 (2007) [arXiv:hep-ph/0702223].
- [10] Z. Thomas, D. Tucker-Smith and N. Weiner, “Mixed Sneutrinos, Dark Matter and the LHC,” arXiv:0712.4146 [hep-ph].
- [11] T. Appelquist, H. C. Cheng and B. A. Dobrescu, “Bounds on universal extra dimensions,” *Phys. Rev. D* **64**, 035002 (2001) [arXiv:hep-ph/0012100].
- [12] H. Georgi, A. K. Grant and G. Hailu, “Brane couplings from bulk loops,” *Phys. Lett. B* **506**, 207 (2001) [arXiv:hep-ph/0012379].
- [13] G. von Gersdorff, N. Irges and M. Quiros, “Bulk and brane radiative effects in gauge theories on orbifolds,” *Nucl. Phys. B* **635**, 127 (2002) [arXiv:hep-th/0204223].
- [14] H. C. Cheng, K. T. Matchev and M. Schmaltz, “Radiative corrections to Kaluza-Klein masses,” *Phys. Rev. D* **66**, 036005 (2002) [arXiv:hep-ph/0204342].

- [15] M. Carena, T. M. P. Tait and C. E. M. Wagner, “Branes and orbifolds are opaque,” *Acta Phys. Polon. B* **33**, 2355 (2002) [arXiv:hep-ph/0207056].
- [16] F. del Aguila, M. Perez-Victoria and J. Santiago, “Bulk fields with general brane kinetic terms,” *JHEP* **0302**, 051 (2003) [arXiv:hep-th/0302023].
- [17] F. del Aguila, M. Perez-Victoria and J. Santiago, “Effective description of brane terms in extra dimensions,” *JHEP* **0610**, 056 (2006) [arXiv:hep-ph/0601222].
- [18] J. A. R. Cembranos, J. L. Feng and L. E. Strigari, “Exotic collider signals from the complete phase diagram of minimal universal extra dimensions,” *Phys. Rev. D* **75**, 036004 (2007) [arXiv:hep-ph/0612157].
- [19] E. Ponton and L. Wang, “Radiative effects on the chiral square,” *JHEP* **0611**, 018 (2006) [arXiv:hep-ph/0512304].
- [20] G. Burdman, B. A. Dobrescu and E. Ponton, “Resonances from Two Universal Extra Dimensions,” *Phys. Rev. D* **74**, 075008 (2006) [arXiv:hep-ph/0601186].
- [21] G. Servant and T. M. Tait, “Is the lightest Kaluza-Klein particle a viable dark matter candidate?,” *Nucl. Phys. B* **650**, 391 (2003) [arXiv:hep-ph/0206071].
- [22] K. Griest and D. Seckel, “Three Exceptions In The Calculation Of Relic Abundances,” *Phys. Rev. D* **43**, 3191 (1991).
- [23] F. Burnell and G. D. Kribs, “The abundance of Kaluza-Klein dark matter with coannihilation,” *Phys. Rev. D* **73**, 015001 (2006) [arXiv:hep-ph/0509118].
- [24] K. Kong and K. T. Matchev, “Precise calculation of the relic density of Kaluza-Klein dark matter in universal extra dimensions,” *JHEP* **0601**, 038 (2006) [arXiv:hep-ph/0509119].
- [25] B. A. Dobrescu, D. Hooper, K. Kong and R. Mahbubani, “Spinless photon dark matter from two universal extra dimensions,” *JCAP* **0710**, 012 (2007) [arXiv:0706.3409 [hep-ph]].
- [26] H. C. Cheng, J. L. Feng and K. T. Matchev, “Kaluza-Klein dark matter,” *Phys. Rev. Lett.* **89**, 211301 (2002) [arXiv:hep-ph/0207125].
- [27] K. R. Dienes, E. Dudas and T. Gherghetta, “Grand unification at intermediate mass scales through extra dimensions,” *Nucl. Phys. B* **537**, 47 (1999) [arXiv:hep-ph/9806292].
- [28] A. J. Buras, M. Spranger and A. Weiler, “The impact of universal extra dimensions on the unitarity triangle and rare K and B decays.” *Nucl. Phys. B* **660**, 225 (2003) [arXiv:hep-ph/0212143].
- [29] A. J. Buras, A. Poschenrieder, M. Spranger and A. Weiler, “The impact of universal extra

dimensions on $B \rightarrow X/s$ gamma, $B \rightarrow X/s$ gluon, $B \rightarrow X/s$ mu+ mu-, $K(L) \rightarrow \pi 0$ e+ e-, and epsilon'/epsilon," Nucl. Phys. B **678**, 455 (2004) [arXiv:hep-ph/0306158].

[30] U. Haisch and A. Weiler, "Bound on minimal universal extra dimensions from anti- $B \rightarrow X/s$ gamma," Phys. Rev. D **76**, 034014 (2007) [arXiv:hep-ph/0703064].

[31] M. Kakizaki, S. Matsumoto, Y. Sato and M. Senami, "Significant effects of second KK particles on LKP dark matter physics," Phys. Rev. D **71**, 123522 (2005) [arXiv:hep-ph/0502059].

[32] M. Kakizaki, S. Matsumoto, Y. Sato and M. Senami, "Relic abundance of LKP dark matter in UED model including effects of second KK resonances," Nucl. Phys. B **735**, 84 (2006) [arXiv:hep-ph/0508283].

[33] M. Kakizaki, S. Matsumoto and M. Senami, "Relic abundance of dark matter in the minimal universal extra dimension model," Phys. Rev. D **74**, 023504 (2006) [arXiv:hep-ph/0605280].

[34] G. Servant and T. M. P. Tait, "Elastic scattering and direct detection of Kaluza-Klein dark matter," New J. Phys. **4**, 99 (2002) [arXiv:hep-ph/0209262].

[35] D. Majumdar, "Detection rates for Kaluza-Klein dark matter," Phys. Rev. D **67**, 095010 (2003) [arXiv:hep-ph/0209277].

[36] V. K. Oikonomou, J. D. Vergados and C. C. Moustakidis, "Direct detection of dark matter rates for various WIMPs," Nucl. Phys. B **773**, 19 (2007) [arXiv:hep-ph/0612293].

[37] D. Hooper and G. D. Kribs, "Probing Kaluza-Klein dark matter with neutrino telescopes," Phys. Rev. D **67**, 055003 (2003) [arXiv:hep-ph/0208261].

[38] G. Bertone, G. Servant and G. Sigl, "Indirect detection of Kaluza-Klein dark matter," Phys. Rev. D **68**, 044008 (2003) [arXiv:hep-ph/0211342].

[39] D. Hooper and G. D. Kribs, "Kaluza-Klein dark matter and the positron excess," Phys. Rev. D **70**, 115004 (2004) [arXiv:hep-ph/0406026].

[40] L. Bergstrom, T. Bringmann, M. Eriksson and M. Gustafsson, "Gamma rays from Kaluza-Klein dark matter," Phys. Rev. Lett. **94**, 131301 (2005) [arXiv:astro-ph/0410359].

[41] L. Bergstrom, T. Bringmann, M. Eriksson and M. Gustafsson, "Two photon annihilation of Kaluza-Klein dark matter," JCAP **0504**, 004 (2005) [arXiv:hep-ph/0412001].

[42] T. Bringmann, "High-energetic cosmic antiprotons from Kaluza-Klein dark matter," JCAP **0508**, 006 (2005) [arXiv:astro-ph/0506219].

[43] A. Barrau, P. Salati, G. Servant, F. Donato, J. Grain, D. Maurin and R. Taillet, "Kaluza-Klein dark matter and galactic antiprotons," Phys. Rev. D **72**, 063507 (2005)

[arXiv:astro-ph/0506389].

[44] A. Birkedal, K. T. Matchev, M. Perelstein and A. Spray, “Robust gamma ray signature of WIMP dark matter,” arXiv:hep-ph/0507194.

[45] H. C. Cheng, K. T. Matchev and M. Schmaltz, “Bosonic supersymmetry? Getting fooled at the LHC,” Phys. Rev. D **66**, 056006 (2002) [arXiv:hep-ph/0205314].

[46] J. L. Feng, A. Rajaraman and F. Takayama, “Superweakly-interacting massive particles,” Phys. Rev. Lett. **91**, 011302 (2003) [arXiv:hep-ph/0302215].

[47] J. L. Feng, A. Rajaraman and F. Takayama, “Graviton cosmology in universal extra dimensions,” Phys. Rev. D **68**, 085018 (2003) [arXiv:hep-ph/0307375].

[48] N. R. Shah and C. E. M. Wagner, “Gravitons and dark matter in universal extra dimensions,” Phys. Rev. D **74**, 104008 (2006) [arXiv:hep-ph/0608140].

[49] S. Matsumoto, J. Sato, M. Senami and M. Yamanaka, “Solving cosmological problem in universal extra dimension models by introducing Dirac neutrino,” Phys. Lett. B **647**, 466 (2007) [arXiv:hep-ph/0607331].

[50] S. Matsumoto, J. Sato, M. Senami and M. Yamanaka, “Relic abundance of dark matter in universal extra dimension models with right-handed neutrinos,” arXiv:0705.0934 [hep-ph].

[51] B. A. Dobrescu and E. Pontón, “Chiral compactification on a square,” JHEP **0403**, 071 (2004) [arXiv:hep-th/0401032].

[52] G. Burdman, B. A. Dobrescu and E. Ponton, “Six-dimensional gauge theory on the chiral square,” JHEP **0602**, 033 (2006) [arXiv:hep-ph/0506334].

[53] R. N. Mohapatra and A. Perez-Lorenzana, “Neutrino mass, proton decay and dark matter in TeV scale universal extra dimension models,” Phys. Rev. D **67**, 075015 (2003) [arXiv:hep-ph/0212254].

[54] K. Hsieh, R. N. Mohapatra and S. Nasri, “Mixed dark matter in universal extra dimension models with TeV scale $W(R)$ and Z' ,” JHEP **0612**, 067 (2006) [arXiv:hep-ph/0610155].

[55] K. Hsieh, R. N. Mohapatra and S. Nasri, “Dark matter in universal extra dimension models: Kaluza-Klein photon and right-handed neutrino admixture,” Phys. Rev. D **74**, 066004 (2006) [arXiv:hep-ph/0604154].

[56] M. Srednicki, R. Watkins and K. A. Olive, “Calculations Of Relic Densities In The Early Universe,” Nucl. Phys. B **310**, 693 (1988).

[57] K. Agashe, A. Falkowski, I. Low and G. Servant, “KK Parity in Warped Extra Dimension,”

arXiv:0712.2455 [hep-ph].

- [58] J. Dunkley *et al.* [WMAP Collaboration], “Five-Year Wilkinson Microwave Anisotropy Probe (WMAP) Observations: Likelihoods and Parameters from the WMAP data,” arXiv:0803.0586 [astro-ph].
- [59] I. Gogoladze and C. Macesanu, “Precision electroweak constraints on universal extra dimensions revisited,” Phys. Rev. D **74**, 093012 (2006) [arXiv:hep-ph/0605207].
- [60] T. Appelquist and H. U. Yee, “Universal extra dimensions and the Higgs boson mass,” Phys. Rev. D **67**, 055002 (2003) [arXiv:hep-ph/0211023].
- [61] J. R. Ellis, A. Ferstl and K. A. Olive, “Re-evaluation of the elastic scattering of supersymmetric dark matter,” Phys. Lett. B **481**, 304 (2000) [hep-ph/0001005].
- [62] G. K. Mallot, “The spin structure of the nucleon,” in *Proc. of the 19th Intl. Symp. on Photon and Lepton Interactions at High Energy LP99* ed. J.A. Jaros and M.E. Peskin, Int. J. Mod. Phys. A **15S1**, 521 (2000). [eConf **C990809**, 521 (2000)] [hep-ex/9912040].
- [63] D. R. Tovey, R. J. Gaitskell, P. Gondolo, Y. Ramachers and L. Roszkowski, “A new model-independent method for extracting spin-dependent cross section limits from dark matter searches,” Phys. Lett. B **488**, 17 (2000) [arXiv:hep-ph/0005041].
- [64] M. C. Smith *et al.*, “The RAVE Survey: Constraining the Local Galactic Escape Speed,” Mon. Not. Roy. Astron. Soc. **379**, 755 (2007) [arXiv:astro-ph/0611671].
- [65] E. I. Gates, G. Gyuk and M. S. Turner, “The Local Halo Density,” Astrophys. J. **449**, L123 (1995) [arXiv:astro-ph/9505039].
- [66] M. W. Goodman and E. Witten, “Detectability of certain dark-matter candidates,” Phys. Rev. D **31**, 3059 (1985).
- [67] J. D. Lewin and P. F. Smith, “Review of mathematics, numerical factors, and corrections for dark matter experiments based on elastic nuclear recoil,” Astropart. Phys. **6**, 87 (1996).
- [68] Z. Ahmed *et al.* (CDMS Collab.) “A Search for WIMPs with the First Five-Tower data from CDMS” (Phys. Rev. Lett in preparation) [arXiv:0802.3530].
- [69] J. Angle *et al.* (XENON Collab.) “First Results from the XENON10 Dark Matter Experiment at the Gran Sasso National Laboratory” Phys. Rev. Lett. **100**, 021303 (2008) [arXiv:0706.0039v2].
- [70] J. Angle *et al.* (XENON Collab.) “Limits on spin-dependent WIMP-nucleon cross-sections from the XENON10 experiment” submitted to Phys. Rev. Lett. (2008) [arXiv:0805.2939].

- [71] H.S. Lee *et al.* (KIMS Collab.) “Limits on WIMP-nucleon cross section with CsI(Tl) crystal detectors” Phys. Rev. Lett. **99**, 091301 (2007) [arXiv:0704.0423]
- [72] E. Behnke *et al.* (COUPP Collab.) “Spin-Dependent WIMP Limits from a Bubble Chamber” Science **319** 933-936 (2008)
- [73] R. W. Schnee *et al.* [The SuperCDMS Collaboration], “The SuperCDMS experiment,” arXiv:astro-ph/0502435.
- [74] P. L. Brink *et al.* [CDMS-II Collaboration], “Beyond the CDMS-II dark matter search: Super-CDMS,” *In the Proceedings of 22nd Texas Symposium on Relativistic Astrophysics at Stanford University, Stanford, California, 13-17 Dec 2004*, pp 2529 [arXiv:astro-ph/0503583].
- [75] A. Datta, K. Kong and K. T. Matchev, “Discrimination of supersymmetry and universal extra dimensions at hadron colliders,” Phys. Rev. D **72**, 096006 (2005) [Erratum-ibid. D **72**, 119901 (2005)] [arXiv:hep-ph/0509246].
- [76] S. P. Martin, “Compressed supersymmetry and natural neutralino dark matter from top squark-mediated annihilation to top quarks,” Phys. Rev. D **75**, 115005 (2007) [arXiv:hep-ph/0703097].
- [77] H. Baer, A. Box, E. K. Park and X. Tata, “Implications of Compressed Supersymmetry for Collider and Dark Matter Searches,” JHEP **0708**, 060 (2007) [arXiv:0707.0618 [hep-ph]].
- [78] C. Savage, P. Gondolo and K. Freese, “Can WIMP spin dependent couplings explain DAMA data, in light of null results from other experiments?,” Phys. Rev. D **70**, 123513 (2004) [arXiv:astro-ph/0408346] and private communication with C. Savage.
- [79] R. H. Helm, “Inelastic and Elastic Scattering of 187-Mev Electrons from Selected Even-Even Nuclei,” Phys. Rev. **104** (1956) 1466.
- [80] S. Yellin, “Finding an Upper Limit in the Presence of Unknown Background,” Phys. Rev. D **66**, 032005 (2002) [arXiv:physics/0203002v2].
- [81] J. Engel, S. Pittel and P. Vogel, “Nuclear Physics Of Dark Matter Detection,” Int. J. Mod. Phys. E **1**, 1 (1992).
- [82] M.T. Ressel, D.J. Dean, “Spin-Dependent Neutralino-Nucleus Scattering for $A \sim 127$ Nuclei,” Phys. Rev. C **56**, 535 (1997) [arXiv:hep-ph/9702290v1].